

KfK 3083
Dezember 1980

Measurements of Velocity and Reynolds Stresses in the Inlet Region of an Eccentric Annulus Using a Dual Hot-Wire Probe

J. Hejna
Institut für Neutronenphysik und Reaktortechnik
Projekt Schneller Brüter

Kernforschungszentrum Karlsruhe

KERNFORSCHUNGSZENTRUM KARLSRUHE
Institut für Neutronenphysik und Reaktortechnik
Projekt Schneller Brüter

KfK 3083

Measurements of Velocity and Reynolds Stresses in the
Inlet Region of an Eccentric Annulus Using a Dual Hot-
Wire Probe

J. Hejna

(delegated from ÚJV, Řež (CSSR) by an IAEA fellowship)

Kernforschungszentrum Karlsruhe GmbH, Karlsruhe

Als Manuskript vervielfältigt
Für diesen Bericht behalten wir uns alle Rechte vor

Kernforschungszentrum Karlsruhe GmbH
ISSN 0303-4003

Abstract

This paper contains the experimental technique to measure the distributions of velocities and Reynolds stresses in the inlet of an eccentric annulus. The procedure and the results of the calibration of the hot-wire probes are discussed. Moreover, the results obtained by the method at the inlet of an eccentric annulus ($x/d_h = 0.05$) are presented.

The experimental technique used in this investigation is shown to give reliable results. Suggestions to improve the technique are discussed.

Messungen der Geschwindigkeit und der Reynoldschen Spannungen im Einlauf eines exzentrischen Ringspalts mit Hitzdrähten

Zusammenfassung

Der Bericht enthält das Verfahren zur Messung von Verteilungen der Geschwindigkeiten und Reynoldschen Spannungen im Einlauf eines exzentrischen Ringspalts. Das Verfahren und die Ergebnisse der Eichung von Hitzdrähten werden beschrieben. Außerdem werden die Meßergebnisse, die mit dieser Methode erhalten wurden, dargestellt.

Es zeigt sich, daß die Meßmethode, die für diese Untersuchung verwendet wurde, vernünftige Ergebnisse erbringt. Vorschläge zur Verbesserung der Technik werden diskutiert.

Table of contents

1. Introduction
2. Test rig and channel geometry
3. Calibration of hot wire probe
 - 3.1 Velocity calibration
 - 3.2 Yaw and pitch factor calibration
 - 3.3 Calibration of X-wire probe
 - 3.4 Influence of the temperature
4. Measurements in the eccentric annulus
 - 4.1 Static pressure measurements
 - 4.2 Total pressure measurements
 - 4.3 Normal wire probe measurements
 - 4.4 Measurements of time mean velocity and Reynolds stresses using a dual hot wire probe
5. Conclusions
6. References
7. Nomenclature

1. Introduction

In the first part of this report the procedure and the results of the calibration are given for a normal wire probe and a dual probe (x-shaped), respectively.

The second part contains the results of measurements performed in the inlet region of an eccentric annulus. The measuring station is about 0,7 mm, i.e. $z/d_h = 0,05$, downstream of inlet edge of the inner rod (Fig.1)

Because of changes of the velocity and mainly the static pressure both in the radial and peripheral directions and in the axial direction it is not possible to measure time-mean velocities using a Prandtl tube. These measurements were therefore divided into measurements of the static pressure and the total pressure, respectively. Corrections for a change of the Reynolds number during the measurement were applied.

For the measurements of the components of the Reynolds stress tensor the measuring setup suggested by Müller /1/ is used. For these measurements the DISA hot wire miniature probes 55P61 were used.

2. Test rig and channel geometry

An air test rig with a circular tube of an inner diameter of $\phi 100,0$ mm was used. At the outlet side of the tube a disc of the diameter $\phi 86,0$ mm was installed with full eccentricity (i.e. $\epsilon=1,0$). The mass flow rate was measured by a standard orifice plate (DIN 1952) placed in the test rig (Fig.2). The detailed channel geometry is given in Tab.1. Because the channel has relatively small dimensions (for example the ratio of the diameter of the X-probe body and the widest gap is 0,157) the measurements were realized only in the range of $-90^\circ \leq \alpha \leq 90^\circ$.

3. Calibration of hot wire probe

The calibration setup is shown in Fig.3.

For immediate record of the output voltages a X-Y recorder was used.

For the calibration and evaluation method the assumption is made that the geometry of the probe is ideal (i.e. both wires have angles of 45°). The measured values of the sensitivity factors are considered.

3.1 Velocity calibration

This calibration is performed with the direction of the flow from the calibration nozzle perpendicular to the wire to be calibrated (i.e. $\alpha=45^\circ$). Because a linearizer was used this calibration is performed only to check the linearisation. One example for a DISA probe 55P61 is given in Fig.7. In all cases the factor $S=1/10$ was used. For the evaluation of the experimental results it is necessary to make a correction for the real temperature according to Eq.12.

3.2 Yaw and pitch factor calibration

The effective cooling velocity acting on the sensor is usually expressed as:

$$U_{\text{cool}}^2 = \frac{E^2}{S^2} = U_{N_1}^2 + k^2 \cdot U_T^2 + h^2 \cdot U_{N_2}^2 \quad (1)$$

where

k - yaw factor

h - pitch factor

(coordinate system see Figs. 4,5 and 6)

For the rotation around the N_2 axis (Fig.4) the equation is valid:

$$\frac{E^2}{S^2} = U_R^2 (\cos^2 \alpha + k^2 \cdot \sin^2 \alpha) \quad (2)$$

and the yaw factor is:

$$k = \sqrt{\frac{\left(\frac{E(\alpha)}{E(\alpha=0)}\right)^2 - \cos^2 \alpha}{\sin^2 \alpha}} \quad (3)$$

The pitch factor calibration can be performed in three ways:

A. Rotation around the N_2 -axis (Fig.5) with $U_g = \text{const.}$

Then for the cooling velocity Eq.(4) is valid:

$$U_{\text{cool}}^2 = \frac{E^2}{S^2} = U_g^2 \left[\cos^2 \sigma_1 (\sin^2 \gamma + k^2 \cos^2 \gamma) + h^2 \cdot \sin^2 \sigma_1 \right] \quad (4)$$

and the pitch factor for $\gamma=45^\circ$ is:

$$h = \sqrt{\left[\left(\frac{E(\sigma_1)}{E(\sigma_1=0)} \right)^2 - \cos^2 \sigma_1 \right] \frac{1+k^2}{2 \cdot \sin^2 \sigma_1}} \quad (5)$$

In this case k is a function of U_R and α :

$$k = k(U_R, \alpha) = k(U_g \cdot \cos \sigma_1; \alpha = 90 - \gamma) \quad (6)$$

B. Rotation around the wire axis (Fig.6)

a. for $U_g = \text{const.}$

$$h = \sqrt{\frac{\left(\frac{E(\sigma_2)}{E(\sigma_2=0)} \right)^2 - \cos^2 \sigma_2}{\sin^2 \sigma_2}} \quad (7)$$

b. for $U_R = \text{const}$. In this case the velocity from the calibration nozzle must be changed according to

$$U_g = \frac{U_R}{\cos \sigma_2} \quad (8)$$

and the pitch factor is evaluated by

$$h = \sqrt{\frac{\left(\frac{E(\sigma_2)}{E(\sigma_2=0)}\right)^2 - 1}{\tan^2 \sigma_2}} \quad (9)$$

Note, that for comparison of the results of the first (A) and the second (B) method Eq.(10) is valid:

$$\tan \sigma_2 = \frac{\tan \sigma_1}{\sin \gamma} \quad (10)$$

Results of the calibrations of one probe are given in Figs. 8, 9, 10 and 11. The results from the yaw calibration are used in the form:

$$k = A + B \cdot U_g + C(U_g) \cdot \alpha \quad (11)$$

The values A, B, C are taken from the calibrations in this way: For each velocity of the calibration the dependence in the range $20^\circ \leq \alpha \leq 70^\circ$ is the second order polynom evaluated by a least square fit method. The dependence on the velocity is used as measured. Because the wire usually is not quite straight, especially the wires of the x-probes, it is not possible to give a simple general equation.

3.3 Calibration of x-wire probe

For a check of the description accuracy of the yaw factors the dependence of the ratio of the output voltages on the yaw angle is plotted in Fig.12. The theoretical relationship (Eq.17) is in excellent agreement with the measured values.

3.4 Influence of the temperature

The correction of the anemometer readings for the influence of the surrounding air temperature is based on the mean velocity measurement, when the mass flow rate was kept constant. In Fig.13 the results are compared with results from unlinearized anemometer readings (/4/) and the results of Bearmann (/3/).

The following equation was used for the correction of the time-mean and RMS values of the anemometer readings, respectively:

$$E(25) = E(t) \cdot \frac{1}{1,3575 - 0,0143 \cdot t \text{ } (\text{°C})} \quad (12)$$

4. Measurements in the eccentric annulus

4.1 Static pressure measurements

The "static" pressure measurements were performed by three static pressure probes of different outer diameter (Fig.14) available in the laboratory.

The difference between the static pressure measured by the probes and the static pressure in the reference static pressure tap (marked R) on the symmetry line of the channel was measured by a MKS Baraton Tpe 170 Pressure Meter. The measuring head has a range of 0÷10 mm Hg. The reading of the static pressure was very sensitive against the axial position of the probe caused by the con-

ditions in inlet region. Changes of about 1/100 mm in axial direction affected the difference head. In spite of this trouble the results from the three probes agree very well. Small differences occur only in the wake near the inner surface. Some results are given together with results of the total pressure measurements in Figs. 15:21. The distribution of the static pressure in the form of lines of constant static pressure is shown in Fig.22.

4.2 Total pressure measurements

The "total" pressure was measured by a Pitot tube again as a difference between total pressure from the Pitot tube and the static pressure in the reference static pressure tap. The results are shown in Fig. 15-21. The evaluated values of the velocity (\bar{U}_{PIT}) are given in Table 2.

4.3 Normal wire probe measurements

The standard normal wire probe DISA55P11 was used for measurements of the mean velocity and the fluctuations (RMS Voltmeter DISA55D35). Because the flow in the inlet region is three-dimensional, the results of the longitudinal velocity differ from the results of classic instrumentation measurements, which is believed to be insensitive on the flow direction mainly in a wake region. For a wire positioned in the peripheral direction, the radial velocity component increases the reading of the anemometer. The same is true for the longitudinal turbulence intensity. It seems, that its level is very low in comparison with developed conditions in a tube. This is caused by the conditions in the inlet. In four radial positions on the symmetry axis, therefore, the longitudinal distribution of the axial velocity and the turbulent intensity were measured (Fig.23). From these results it follows that the intensity significantly changes downstream from the inlet edge.

4.4 Measurements of time mean velocity and Reynolds stresses using a dual hot wire probe

The velocity fluctuation measurements were performed in the plane of the channel symmetry line in the axial direction, i.e.

$$\alpha = 0$$

and $x/d_h = 0,0143 \pm 0,550$.

The flow direction was measured in this plane in the axial direction and in the circumferential direction for $-90^\circ \leq \alpha \leq +90^\circ$. The measuring setup and switch connections are given in Figs.24 and 25. The scheme of the coordinate systems is shown in Fig.26.

The modified method described in /1/ is used. It is necessary to note that for a check of the method the probe is rotated from $\psi = 0$ to 360° , but only four positions are necessary for the evaluation of all components of the time mean velocity and Reynolds stresses. The average from $\psi = 0 \pm 135^\circ$ and $\psi = 180^\circ \pm 315^\circ$ is considered as the final result. The transfer function for the instantaneous output of the linearized anemometer (wire in position ψ) is given by equation

$$\frac{E^2(\psi)}{S^2} = \bar{U}^2 \cdot m + \bar{V}^2 (\bar{m} \cdot \sin^2 \psi + h^2 \cdot \cos^2 \psi) + \bar{W}^2 (\bar{m} \cdot \cos^2 \psi + h^2 \cdot \sin^2 \psi) - \left\{ \begin{array}{l} \bar{U}\bar{V} \cdot p \cdot \sin \psi - 2 \bar{U} \cdot \bar{W} \cdot p \cdot \cos \psi + 2 \bar{V} \cdot \bar{W} \cdot \sin \psi \cos \psi (\bar{m} - h^2) + \\ + u (2 \bar{U} \cdot m - 2 \bar{V} \cdot p \cdot \sin \psi - 2 \bar{W} \cdot p \cdot \cos \psi) + \\ + v (-2 \bar{U} \cdot p \cdot \sin \psi + 2 \bar{V} (\bar{m} \cdot \sin^2 \psi + h^2 \cdot \cos^2 \psi) + \\ + 2 \bar{W} \cdot \sin \psi \cdot \cos \psi (\bar{m} - h^2)) + \\ + w (-2 \bar{U} \cdot p \cdot \cos \psi + 2 \bar{V} \cdot \sin \psi \cos \psi (\bar{m} - h^2) + \\ + 2 \bar{W} (\bar{m} \cdot \cos^2 \psi + h^2 \cdot \sin^2 \psi)) + \\ + u^2 \cdot m + v^2 (\bar{m} \cdot \sin^2 \psi + h^2 \cdot \cos^2 \psi) + w^2 (\bar{m} \cdot \cos^2 \psi + h^2 \cdot \sin^2 \psi) - \\ - 2uv \cdot p \cdot \sin \psi - 2uw \cdot p \cdot \cos \psi + 2vw \cdot (\bar{m} - h^2) \sin \psi \cos \psi. \end{array} \right\} \begin{array}{l} \bar{F}^2 \\ f \\ g \end{array} \quad (13)$$

and can be written as

$$\frac{E^2(\psi)}{S^2} = \bar{F}^2 + f + g \quad (14)$$

The following assumptions are made:

$$\frac{\bar{E}_k}{S} = \bar{F}_k \quad \text{for the time mean value} \quad (15)$$

and $\frac{e_k^2}{s^2} = \frac{f_k^2}{4 \cdot F_k^2}$; or $\frac{(e_k \pm e_{k+4})^2}{s^2} = \left[\frac{f_k}{2F_k} \pm \frac{f_{k+4}}{2F_{k+4}} \right]^2$ (16)

for the fluctuations

The following procedure is applied:

a. Flow direction measurement

The probe is rotated around its axis in steps of 45 deg and only the time mean output voltages from both wires are read. In the position where the ratio of output voltages is maximal or minimal the transverse velocity vector is parallel with the plane of the wire and prongs. Then the angle of rotation (ψ_D) for the minimum and maximum value of \bar{E}_1/\bar{E}_2 is calculated by a computer program for evaluation of the results. The angle ϕ between the probe axis and the velocity vector is evaluated from the equation:

$$\operatorname{tg}^2 \phi + 2 \cdot \operatorname{tg} \phi \cdot \frac{E^*^2 \cdot p_2 + p_1}{E^*^2 \cdot m_2 - m_1} + \frac{E^*^2 \cdot m_2 - m_1}{E^*^2 \cdot m_2 - m_1} = 0 \quad (17)$$

where

$$E^* = \frac{E_1}{E_2}$$

$$m_{1,2} = \sin^2 \gamma_{1,2} + k_{1,2}^2 \cdot \cos^2 \gamma_{1,2}$$

$$\bar{m}_{1,2} = \cos^2 \gamma_{1,2} + k_{1,2}^2 \cdot \sin^2 \gamma_{1,2} \quad (18)$$

$$p_{1,2} = \sin \gamma_{1,2} \cdot \cos \gamma_{1,2} (1 - k_{1,2}^2)$$

and the indices 1,2 are related to the first or second wire of the x-probe, respectively.

The value of the yaw factor is computed from the calibration of each wire:

$$\begin{aligned} k_1 &= k_1(\bar{U}, \alpha_1) \\ k_2 &= k_2(\bar{U}, \alpha_2) \end{aligned} \quad (19)$$

where $\alpha_1 = 90 - \gamma_1 + \phi$
 $\alpha_2 = 90 - \gamma_2 - \phi$

The absolute value of the axial velocity \bar{U} is calculated for both wires and both positions of the probe (i.e. ψ_D for minimal and maximal value of E^*) according to Eq. 20:

$$\bar{U} = \frac{\bar{E}_{1,2}^2 / s^2}{m_{1,2} + \bar{m}_{1,2} \cdot \tan^2 \phi - 2 \cdot p_{1,2} \cdot \tan \phi} \quad (20)$$

The velocities are then recalculated to the polar laboratory coordinates (y, α, x) (see Fig. 27). The results of the flow direction measurements from both wires and at both positions (max and min) agree very well. Averaged values of the transverse velocity related to the longitudinal velocity are given in the Tab. 2 and Figs. 28÷30.

The results show good agreement between the two symmetrical halves of the channel (Fig. 28) and essentially the same distribution of the relative transverse velocity along the normal to the inner wall. Fig. 31 and Tab. 3 show the development of the flow direction in axial direction on the channel symmetry line.

The distribution of the axial velocity is given in Tab. 2 and Fig. 32÷35. The stability of both the linearisator and bridge is not high enough to give absolute values of high accuracy. Therefore the hot-wire method is not sufficient for high accuracy without permanent calibration.

The values of the relative transverse velocities especially in the surrounding of the inner wall are very high and the flow direction is away from this wall. In the surrounding of the outer wall the transverse velocity is relatively weak and the direction is towards the symmetry line of the channel.

b, Reynolds stresses

From the position of the minimal value of E^* the measurements of the Reynolds stresses are started.

The values of \overline{E}_k , $\overline{e_k^2}$, $\overline{(e_k+e_{k+4})^2}$ and $\overline{(e_k-e_{k+4})^2}$ (see Eq.12) at each position of the probe ($k = 1 \div 8$, $k = 9 \equiv k=1$ for a check; $\psi = (k-1) \cdot \frac{\pi}{4}$) are read. The coefficients of the resulting set of equations (21) are given in Tabs. 4 and 5.

$$\frac{\overline{e_k^2}}{s^2} = a_{i,j}(\psi_k) \cdot \overline{u_i u_j}; \quad i=1 \div 3, j \geq i \quad (21)$$

$$\frac{\overline{(e_k+e_{k+4})^2}}{s^2} = b_{i,j}(\psi_k) \cdot \overline{u_i u_j}$$

where

$$\begin{aligned} n_{k,k+4} &= \sqrt{m_k} + \sqrt{m_{k+4}}; & \bar{n}_{k,k+4} &= \sqrt{m_k} - \sqrt{m_{k+4}} \\ q_{k,k+4} &= \frac{p_k}{\sqrt{m_k}} + \frac{p_{k+4}}{\sqrt{m_{k+4}}}; & \bar{q}_{k,k+4} &= \frac{p_{k+4}}{\sqrt{m_{k+4}}} - \frac{p_k}{\sqrt{m_k}} \\ m_k &= \sin^2 \gamma_k + \cos^2 \gamma_k \\ p_k &= \sin \gamma_k \cdot \cos \gamma_k (1 - k^2) \end{aligned} \quad (22)$$

For the solution of these equations the following assumption is made:

$$\begin{aligned} \gamma_1 &= \gamma_2 = 45^\circ \\ k &= 0. \end{aligned} \quad (23)$$

Some of these equations are chosen and three sets of equations are compiled. From each set of equations it is possible to calculate the second order fluctuations and the average value of the three results is taken as the final result.

Because the time mean velocity vector is not parallel with the probe axis as in the original method of Müller /1/ due to the geometry of closed channels, it is necessary to perform measurements in all eight positions of the probe and the results must be averaged. In the last step the correlations are recalculated from the coordinates of the measurement arrangement to the laboratory coordinates. All turbulent intensities are related to the friction velocity on the outer wall. The results of measurements along the symmetry line of the channel ($\alpha = 0^\circ$, $x/d_h = 0,05$) are given in Tab.6 and Fig. 36-38.

The results show that in the surrounding of the outer wall the flow is nearly homogeneous, it means that the turbulence intensities are the same in all directions and the correlations are very small, practically zero. The development of the turbulence intensities along the x-axis are shown in Tab.7 and Fig.39-44.

5. Conclusions

There are only few experimental results in the literature for comparison with the new results. All experiments, available in the literature (e.g. /6/) have other inlet conditions. These conditions have a very strong influence on the turbulence intensities. The same is valid for very short distances of the measuring station from the inlet.

Following general statements can be made on the results and the method of this investigation.

1. The results of the measurements of the velocity direction have good accuracy and reproducibility. The measurement of nearly longitudinal flows is affected by the nonexactness of fabrication of the x-probe. It is possible to improve the results by the use of a more exact and more reliable traversing mechanism in the calibration device and by selection of the probes used.
2. To improve the method it is necessary to remove the assumption $k = 0$ and to solve the equations given in the Tabs. 4 and 5. In the next step corrections for turbulence intensities in the evaluation of the time mean velocities should be introduced.
3. The basis of this method - the measurement of the squared RMS value and its sum or difference from two wires simultaneously gives the possibility to measure all turbulence intensities and correlations of the second order and to remove largely the influences of the temperature and the fluctuations of the flow rate.

Acknowledgements:

I appreciate very much the useful discussions with Dr. Rehme, the support of the laboratory staff, especially by Mr. Mensinger and the typing of the manuscript by Mrs. Stassen.

6. References

/1/ Müller, U.:

Messung von Reynoldsschen Spannungen und zeitlich gemittelten Geschwindigkeiten in einer dreidimensionalen Grenzschicht mit nichtverschwindenden Druckgradienten. Ph.D. thesis, Rheinisch-Westfälische Technische Hochschule, Aachen, (1979).

/2/ Rehme, K.:

Untersuchungen der Turbulenz- und Schubspannungsverteilung an einem Kreisrohr mit einem Hitzdraht-Anemometer. Report KfK-1642, (1972)

/3/ Bearman, P.W.:

Corrections for the effect of ambient temperature drift on hot-wire measurements in incompressible flow, DISA Information No.11 - May 1971

/4/ Hejna, J., Mantlik, F.:

Results of the thermoanemometric calibration experiments (transl.) Report ÚJV 3871-R, 1976.

/5/ Jørgensen, F.E.:

Directional sensitivity of wire and fiber-film probes.
DISA Information No.11 - May 1971

/6/ Volnistova, Gabrianovich, Levchenko, Trubakov;

Report FEI - 725, Obninsk 1976

7. Nomenclature

A, B, C	-	empirical constants in Eq. (11)
d	m	diameter of the static pressure taps of the static pressure probe
d_h	m	hydraulic diameter
D	m	diameter of the static pressure and the total pressure probes, respectively
D_1, D_2	m	diameter of the inner and outer surfaces of an eccentric annulus, respectively
e	v	RMS value of the anemometer reading
E, \bar{E}	v	time mean value of the anemometer reading
F, f, g	-	functions, def. by Eq. (15)
h	-	pitch factor
k	-	yaw factor
k	-	number of the wire positions
k'	$m^2 \cdot s^{-2}$	turbulence intensity
p_{st}	Pa	static pressure
p_{tot}	Pa	total pressure
m, \bar{m}, p	-	functions, def. by Eq.(18)
n, \bar{n}, q, \bar{q}	-	functions, def. by Eq.(22)
t	$^{\circ}C$	temperature
u, v, w	$m \cdot s^{-1}$	velocity fluctuation in the axial, radial and peripheral directions, respectively
u', v', w'	-	RMS value of u, v, w
$\bar{U}, \bar{V}, \bar{W}$	$m \cdot s^{-1}$	time mean velocity in the axial, radial and peripheral directions, resp.
U_c	$m \cdot s^{-1}$	absolute value of the velocity vector
U_g, U_R	$m \cdot s^{-1}$	resulting velocities, def. in Fig.4,5 and 6
\bar{V}_{TR}	$m \cdot s^{-1}$	traverse velocity
v^*	$m \cdot s^{-1}$	friction velocity on the outer wall
S	$V / (m \cdot s^{-1})$	transfer constant of the linearization
y	m	distance from the wall
y_{max}	m	distance between inner and outer walls
α, β	-	angles of the position of the probes
γ	-	angle of the inclination of the slanting wire
ϕ	-	angle between the probe axis and the velocity vector \bar{U}_c in the plane of the wire and prongs
ψ_D	-	angle of the rotation of the probe
ψ	-	angle of the position of the wire
α, σ	-	yaw and pitch angles, def. in Fig.4,5 and 6, resp.
θ	-	overheating ratio

Subscripts

D	X-wire probe in the position ψ_D
1,2	number of the wire
f1	flow meter
bar	barometric (of the surrounding air)
R	reference static pressure tap

Coordination system (see Figs. 26 and 27)

x, y, z	}	laboratory systems
r, α, z		
x_2, y_2, z_2		probe system
N_1, T, N_2		wire system

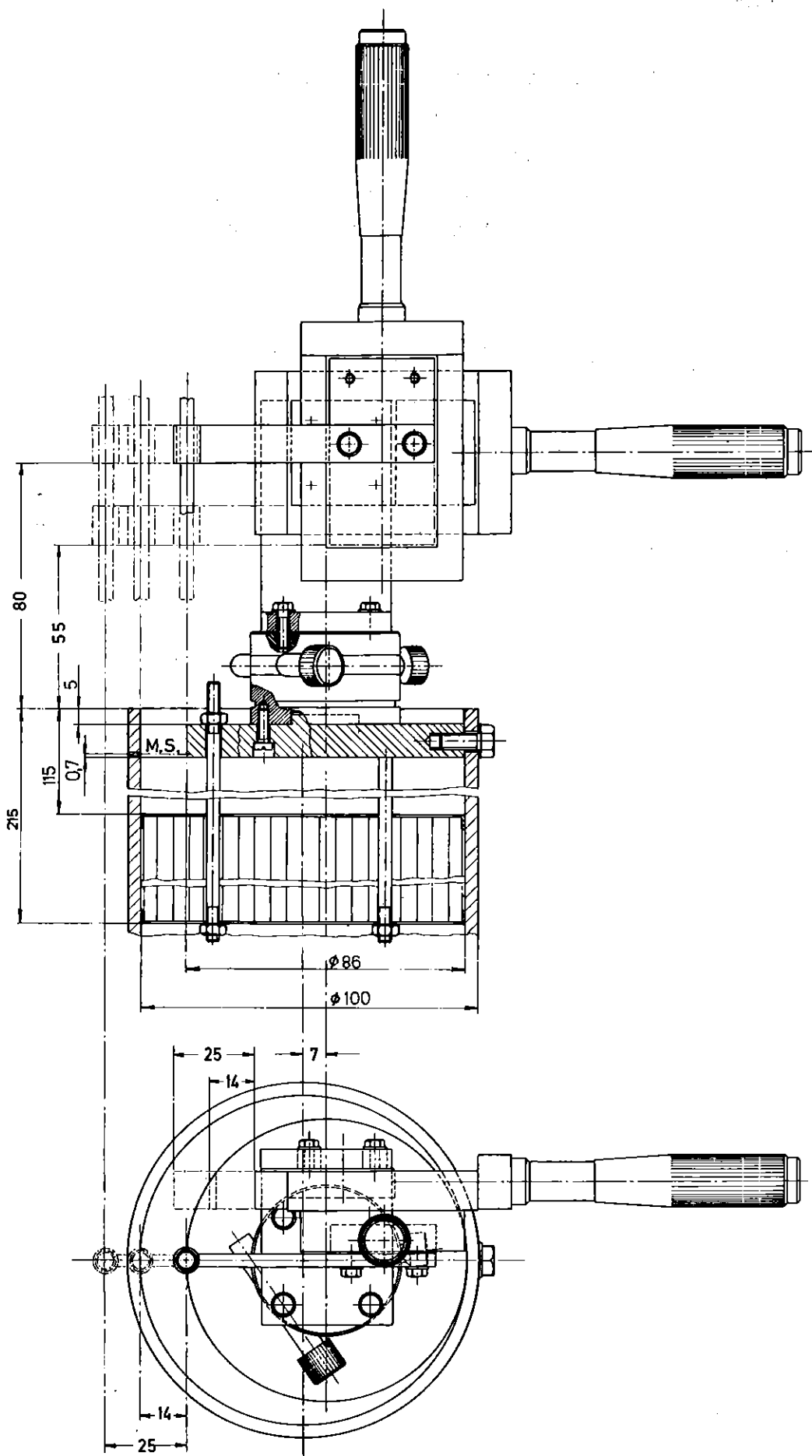
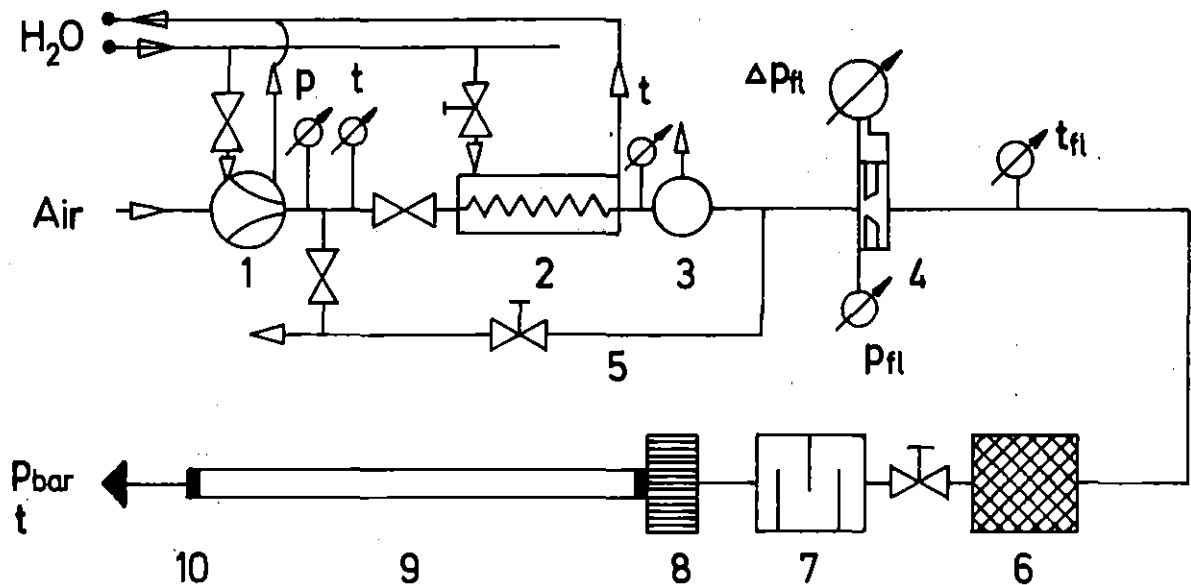


Fig.1: Scheme of the traversing mechanism and the arrangement of the measuring station



1. Compressor
2. Aircooler
3. Water separator
4. Flowmeter
5. By-pass
6. Filter
7. Sound damper
8. Rectifier
9. Circular tube
10. Measuring station (See Fig. 1)

Δp_{fl} Pressure difference
 p_{fl} Pressure before flowmeter
 t_{fl} Air temp. at flowmeter
 P_{bar} Barometric pressure

Fig.2: Scheme of the test rig

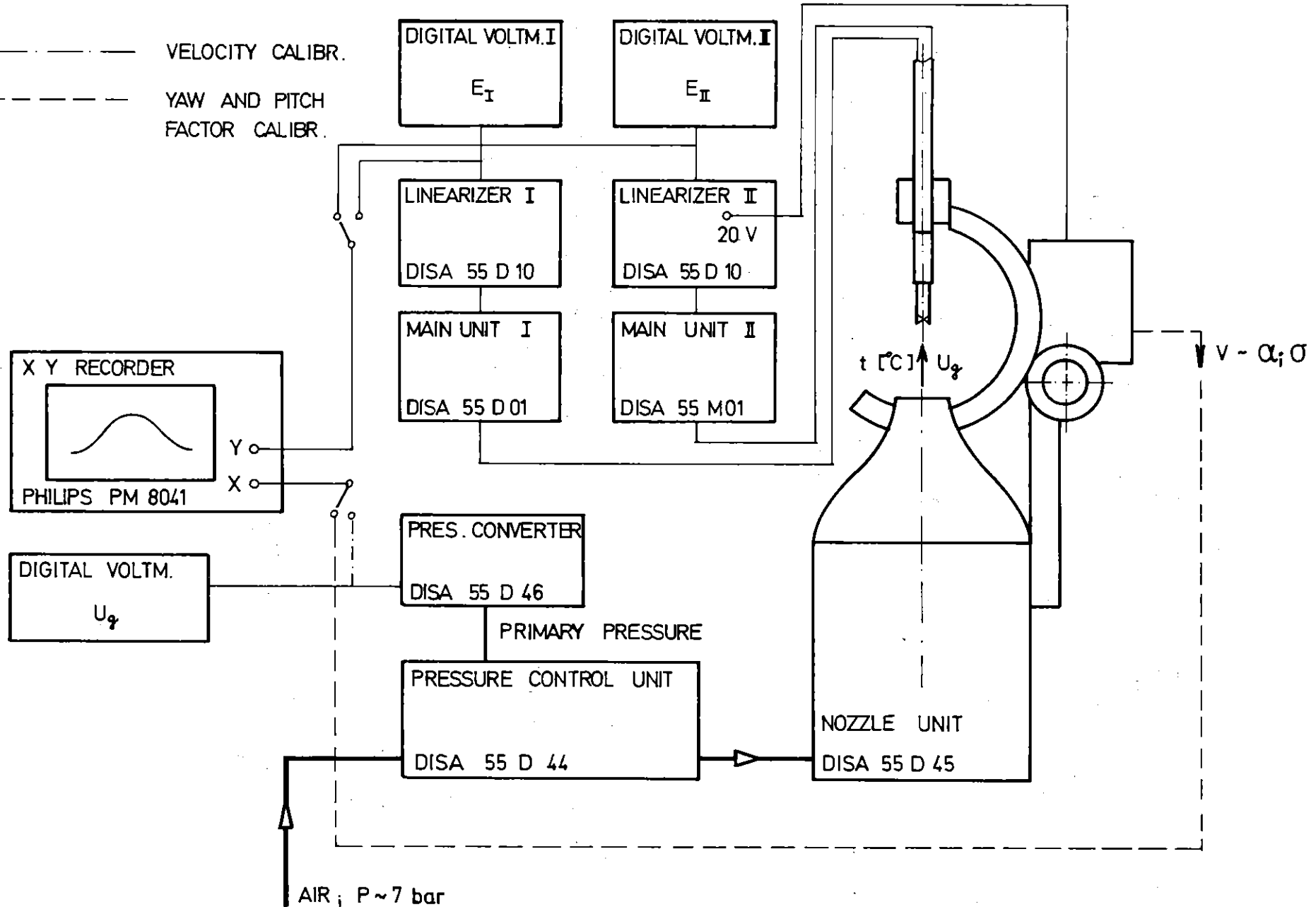


Fig.3: Arrangement of the calibration

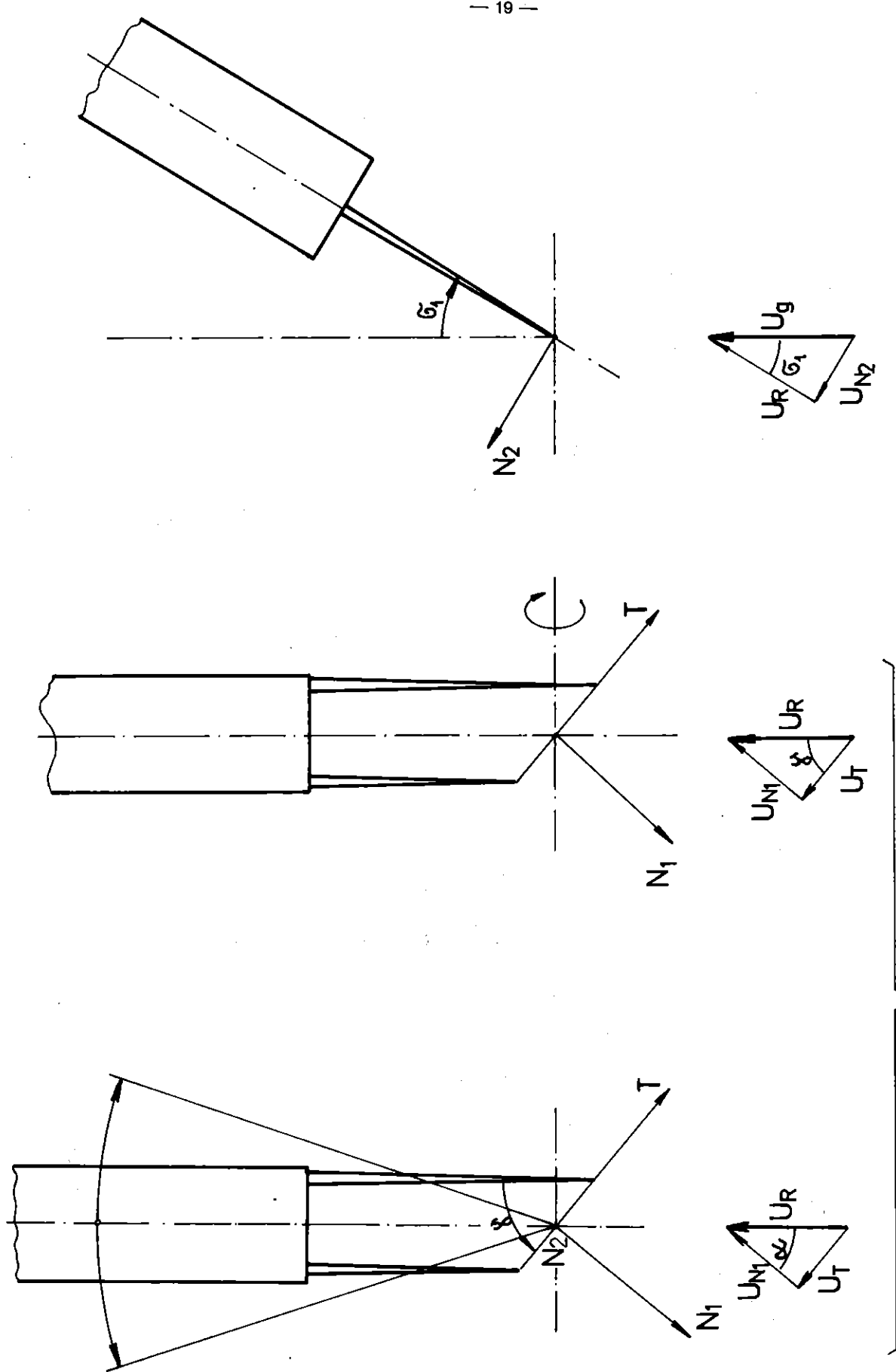


Fig.4: Calibration of yaw sensitivity

Fig.5: Calibration of pitch sensitivity

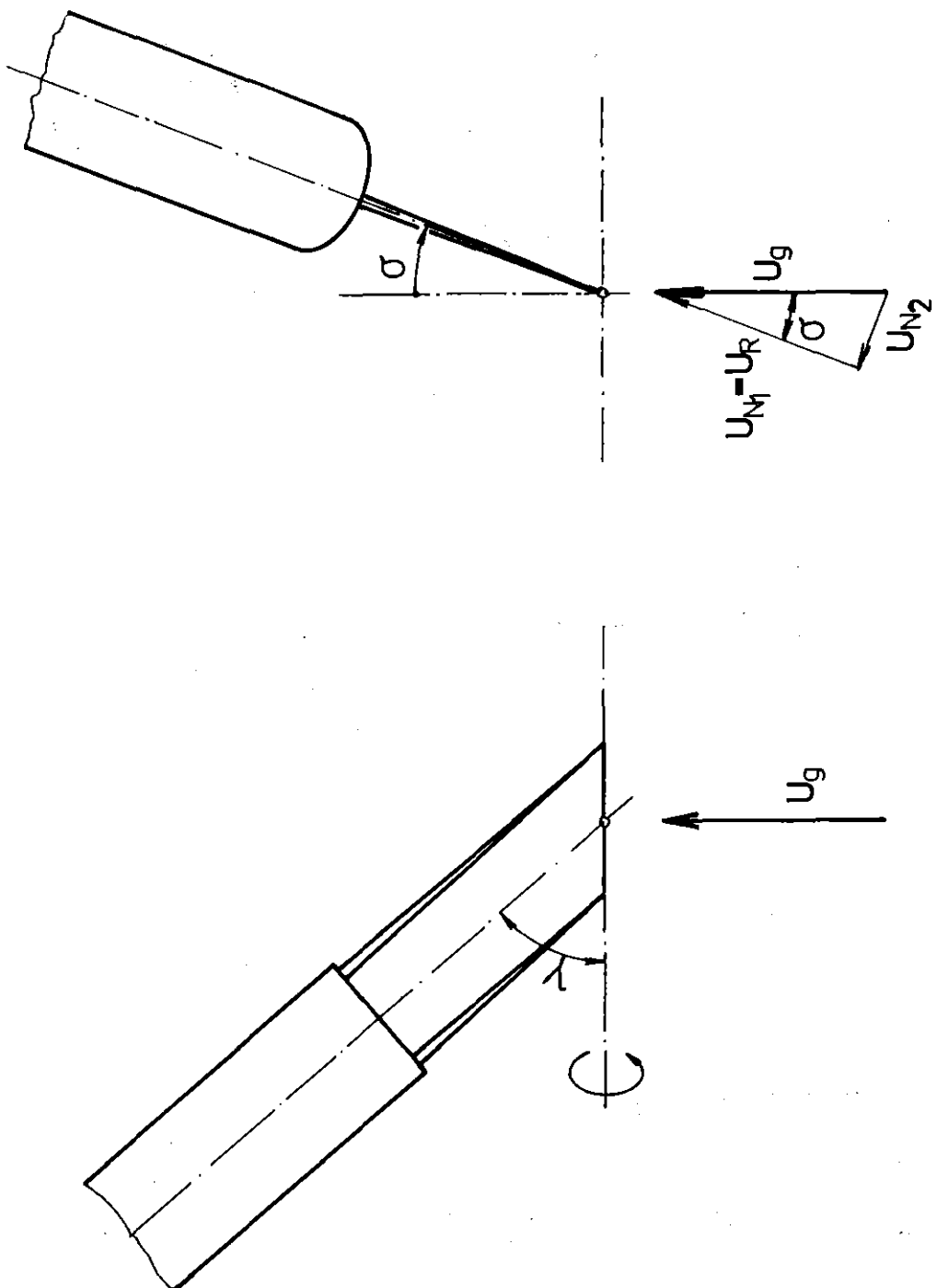


Fig. 6: Calibration of pitch sensitivity

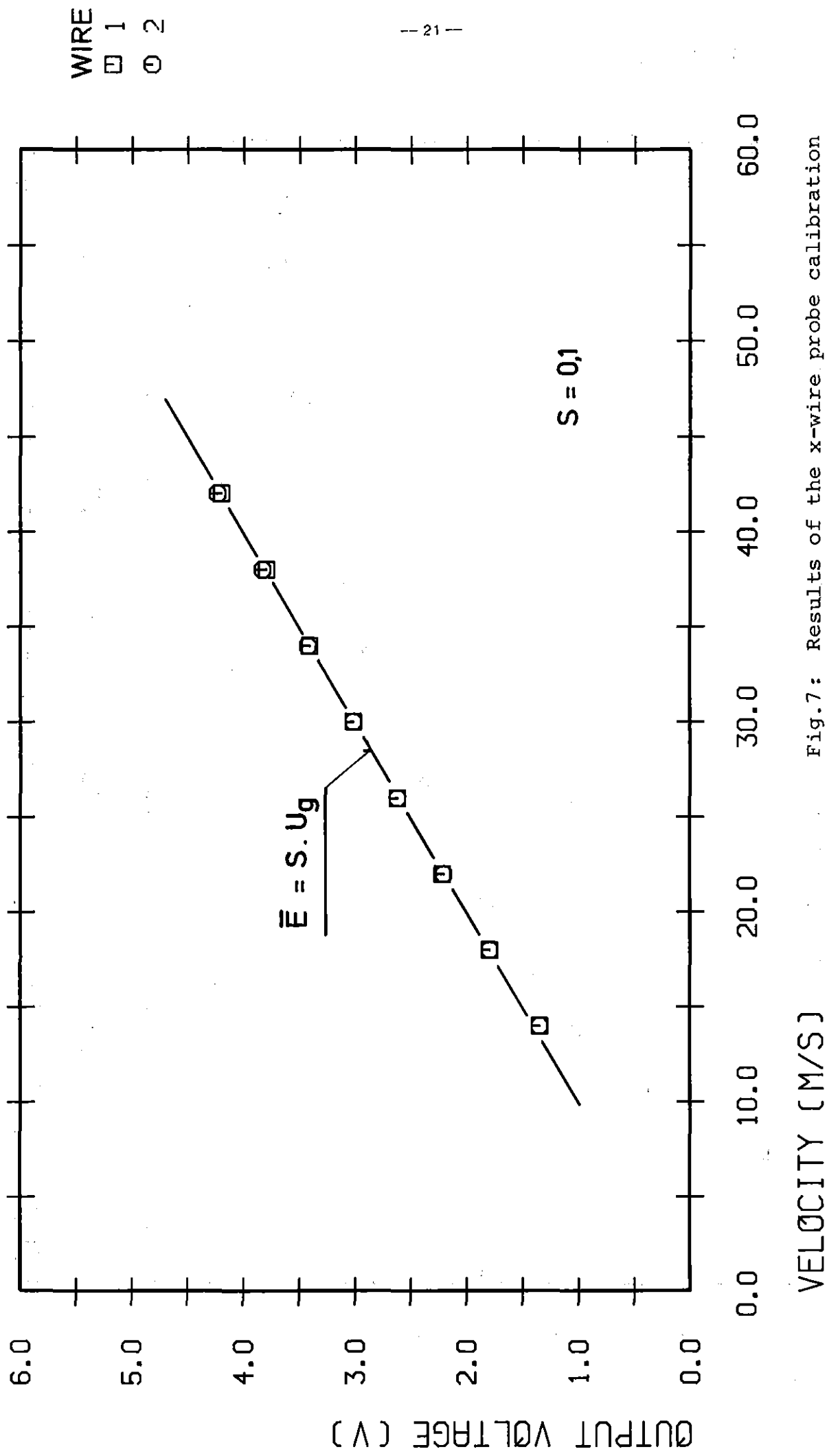


Fig. 7: Results of the x-wire probe calibration

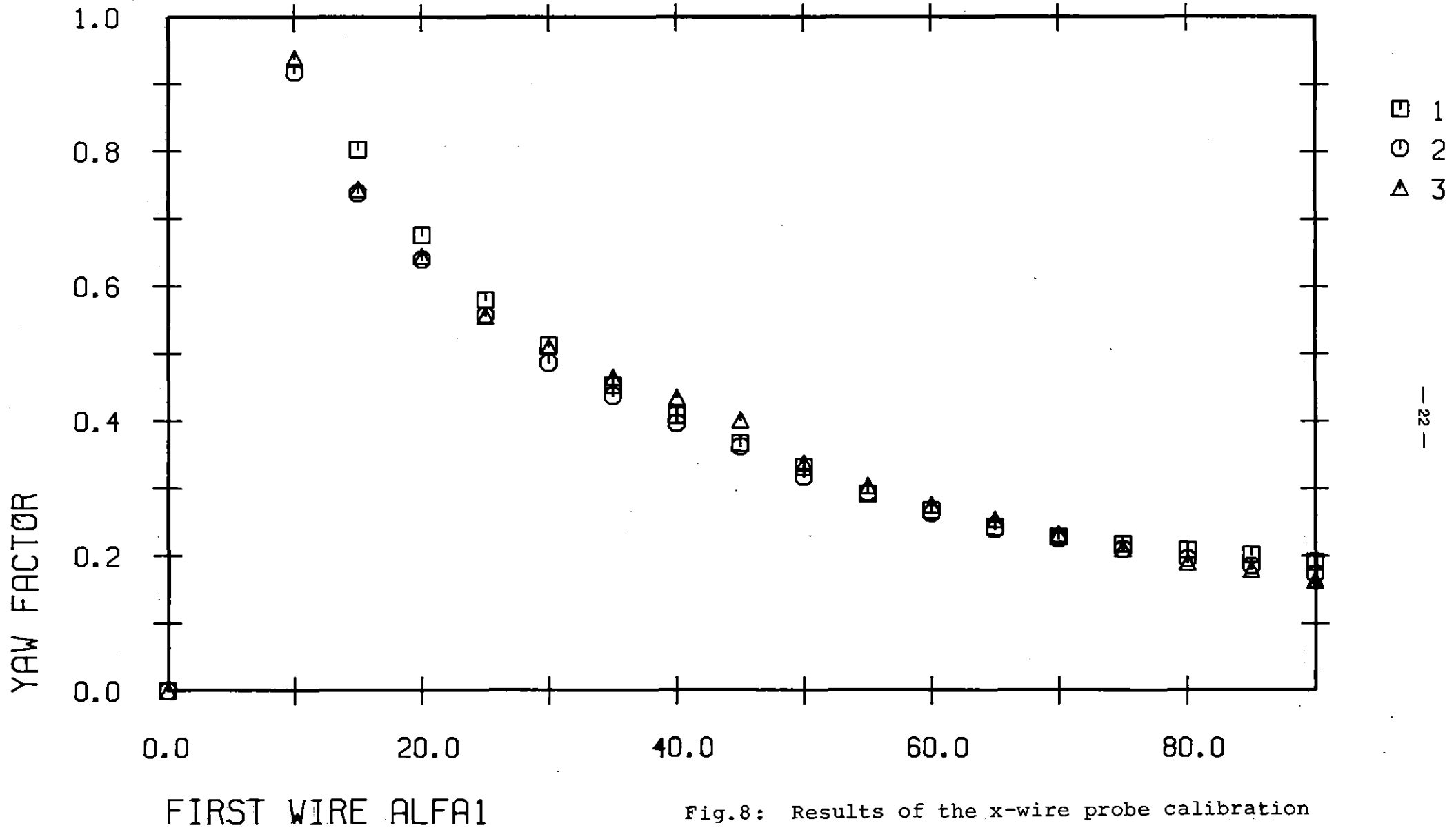
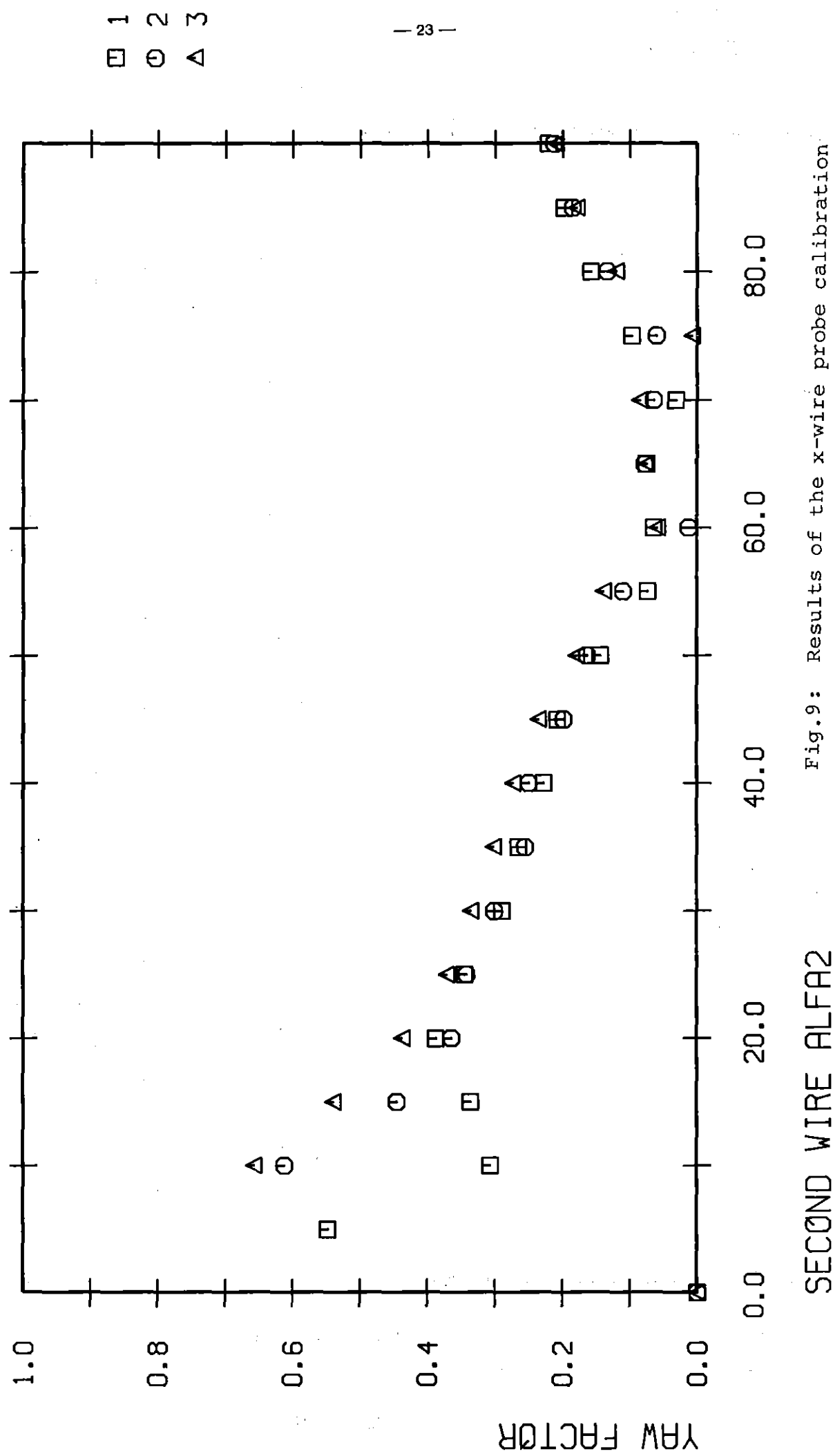


Fig.8: Results of the x-wire probe calibration



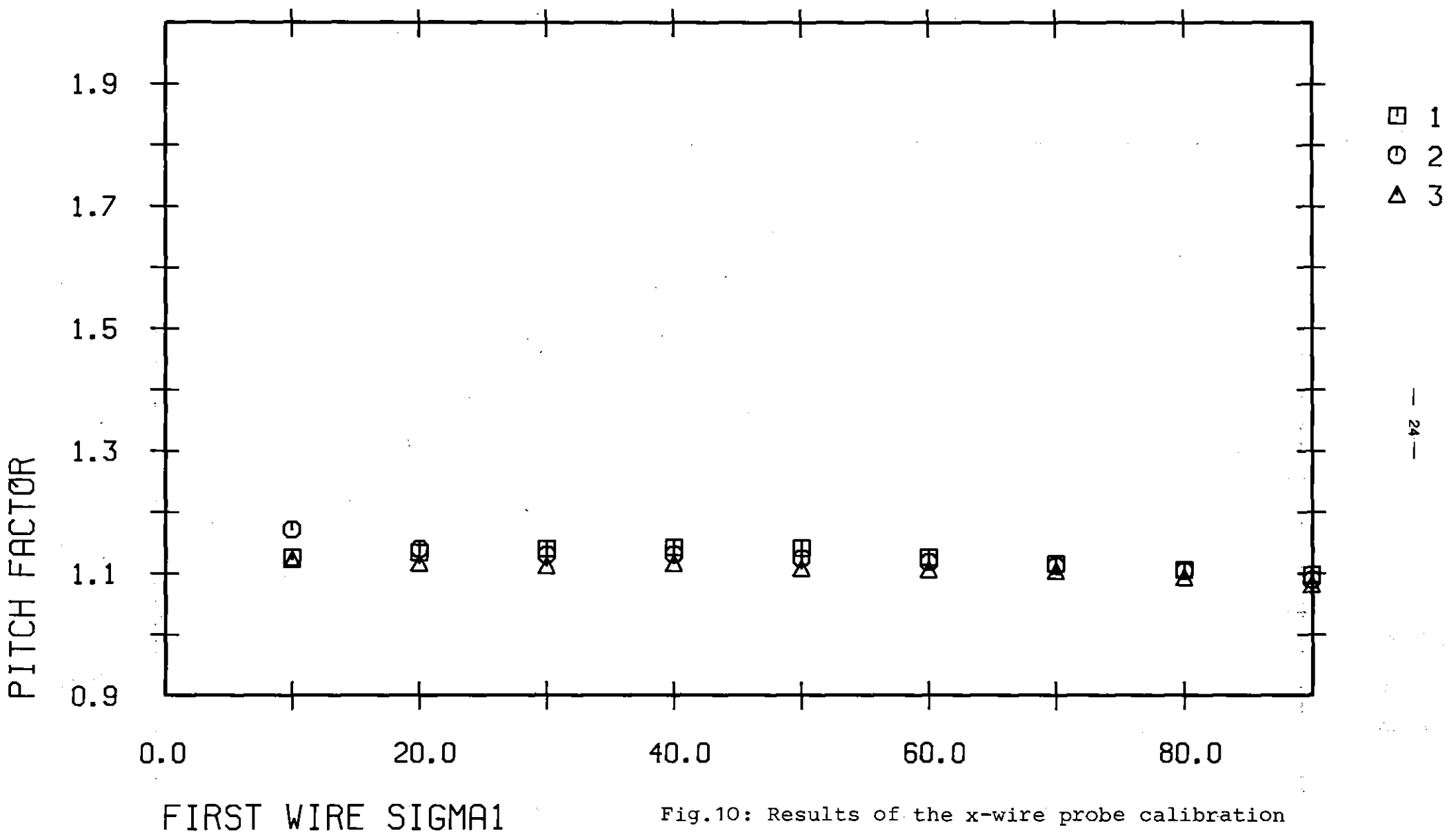


Fig.10: Results of the x-wire probe calibration

PITCH FACTOR

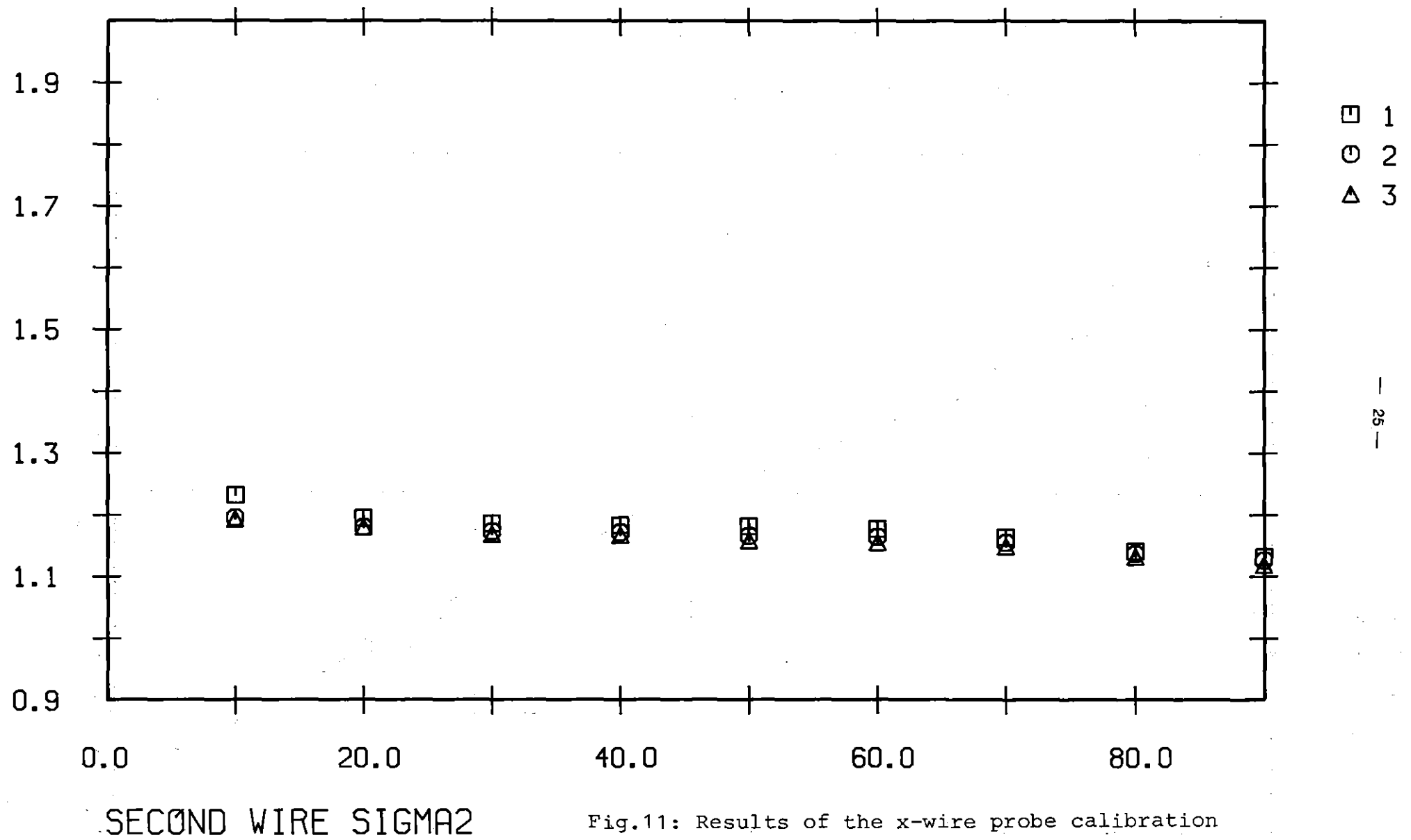


Fig.11: Results of the x-wire probe calibration

OUTPUT VOLTAGE RATIO

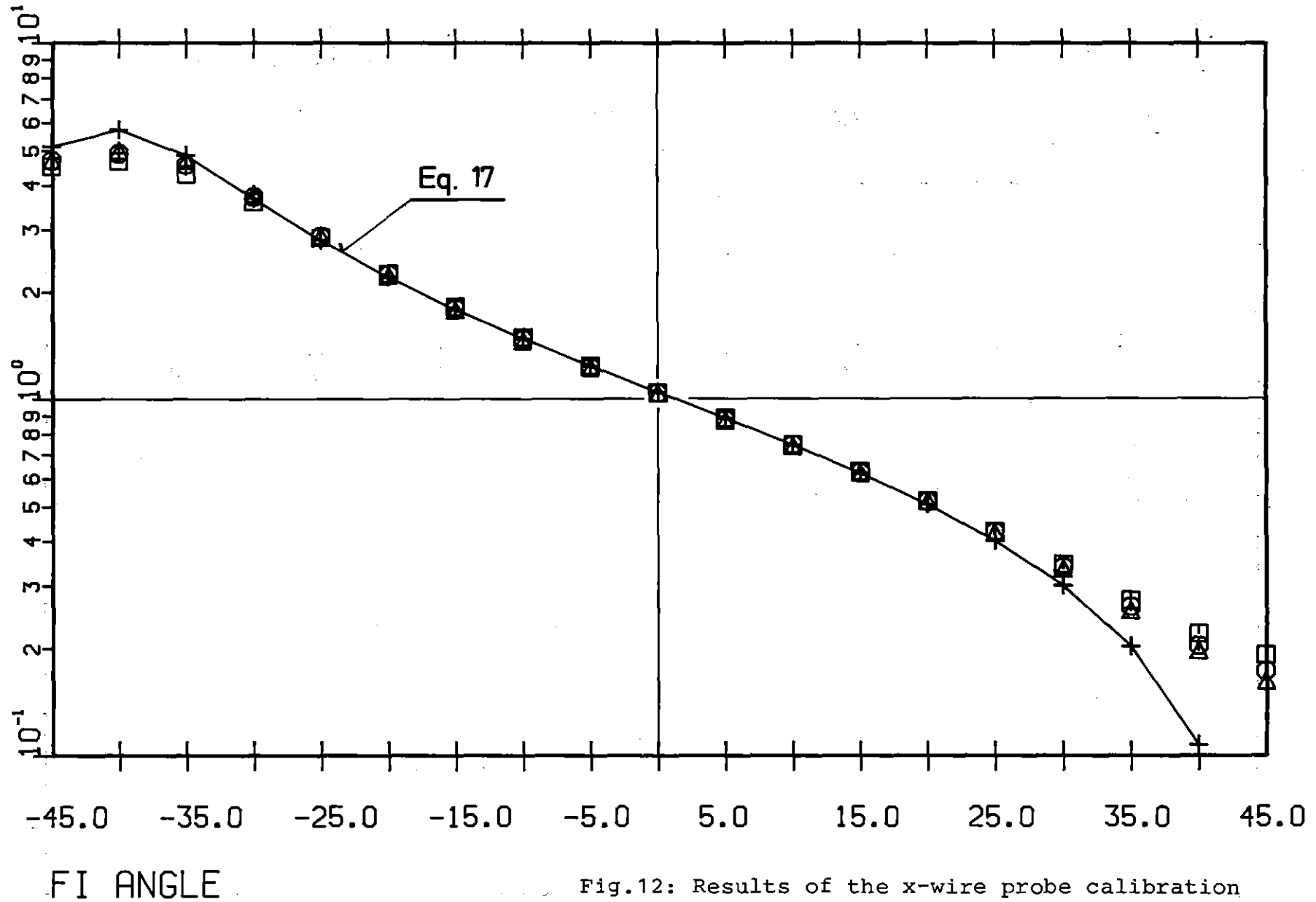


Fig.12: Results of the x-wire probe calibration

— 26 —
□ Θ △ +

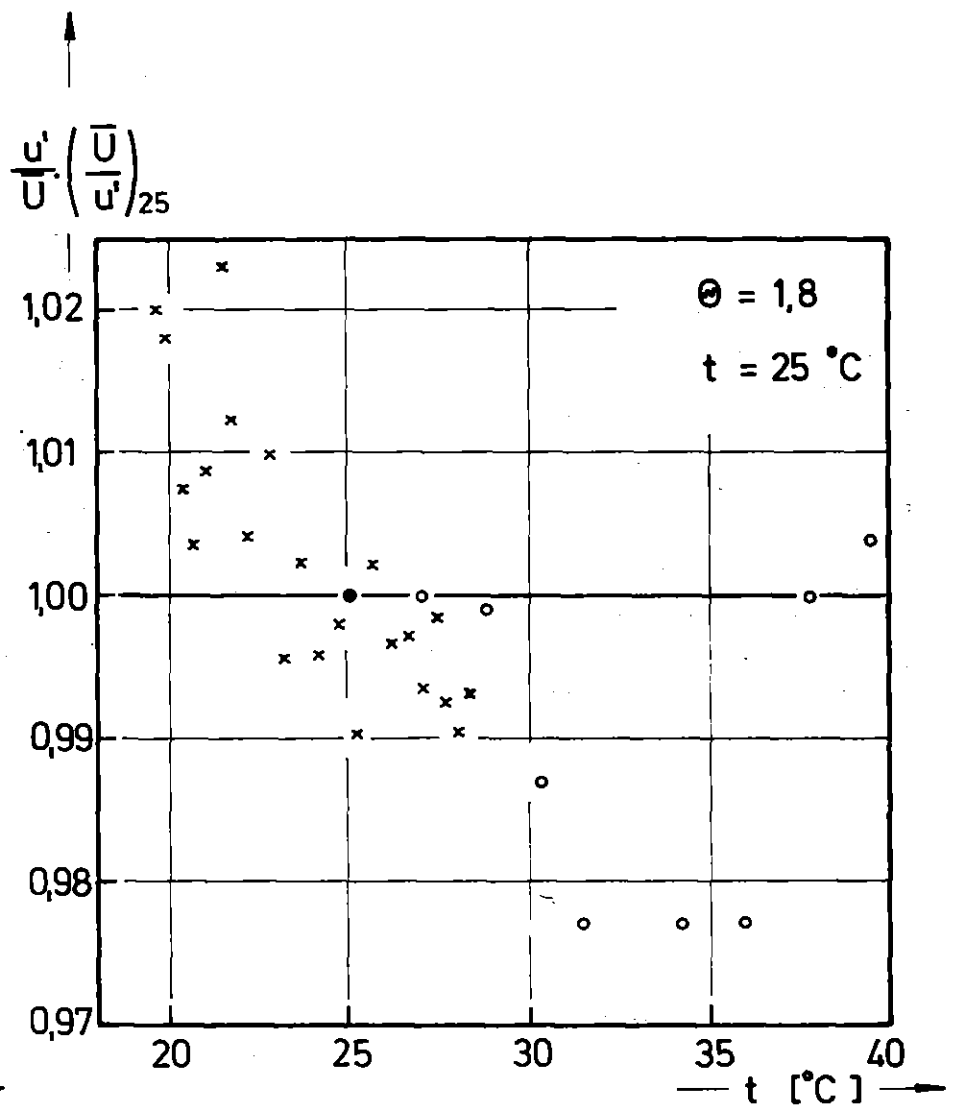
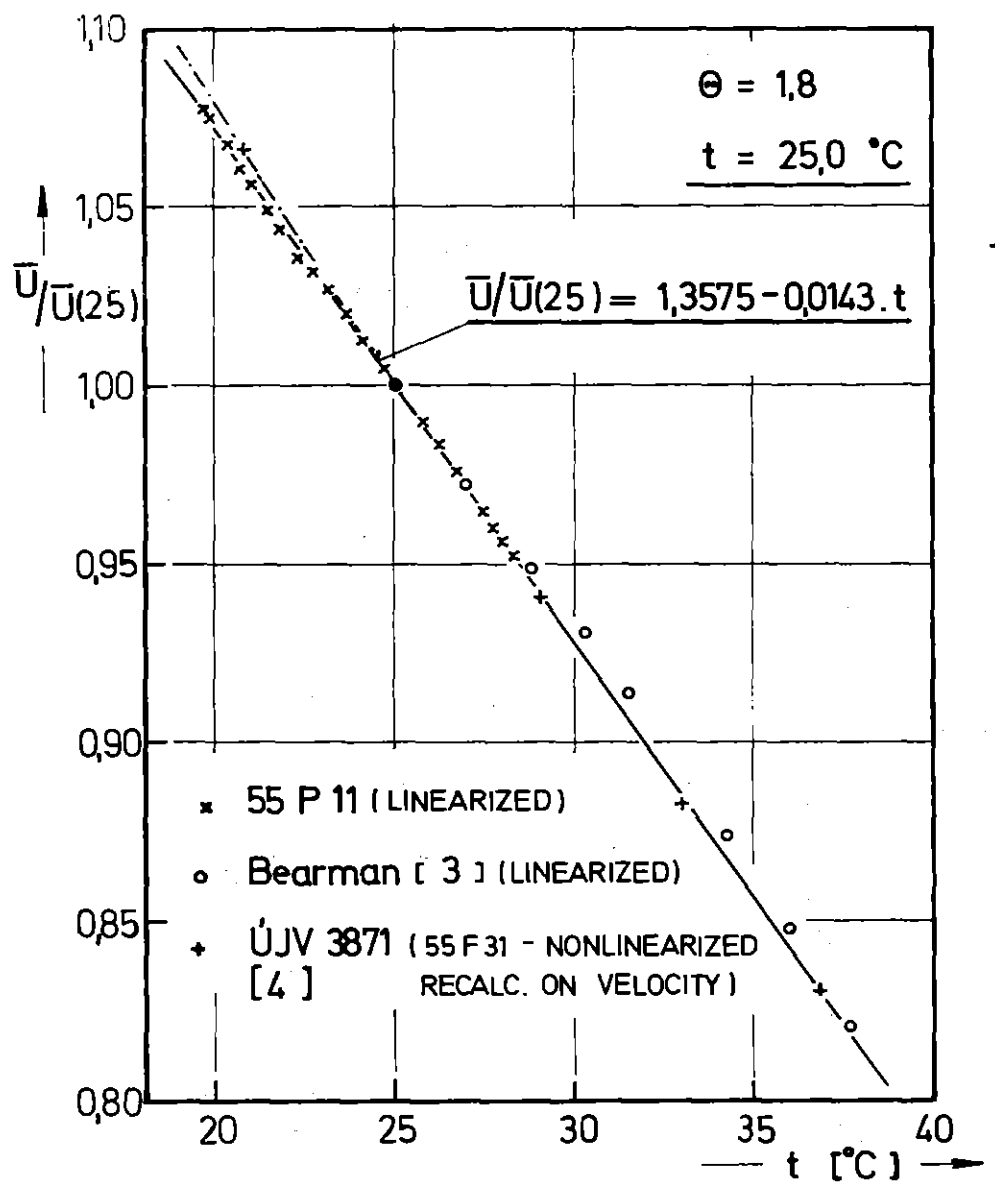
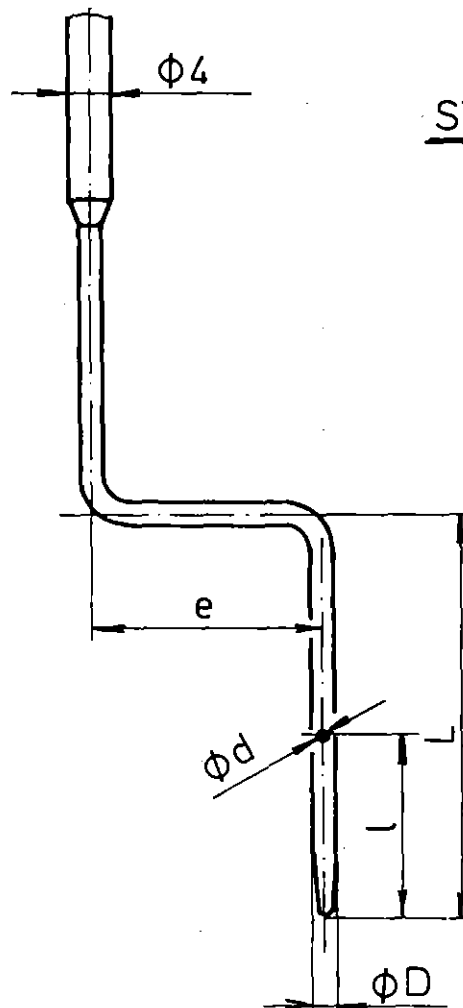
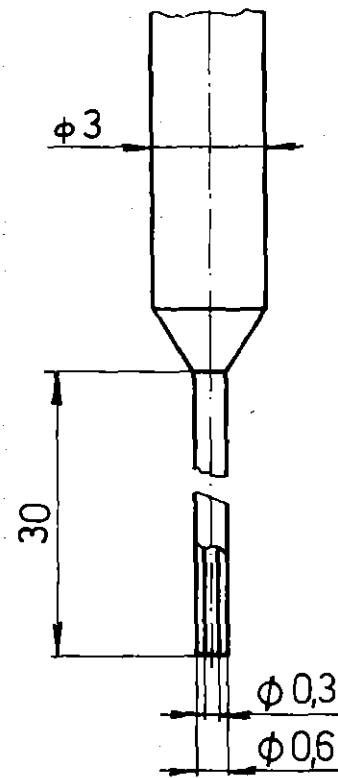


Fig. 13: Influence of the temperature on the anemometer reading

PITOT TUBE



STATIC PRESSURE PROBES

PROBE No.	1	2	3
D	1,60	1,00	0,60
d	~0,15	~0,15	~0,10
e	~26,0	30,5	21,0
l	13,0	7,0	5,8
L	30,5	23,3	18,0

Fig.14: Static pressure and total pressure probes

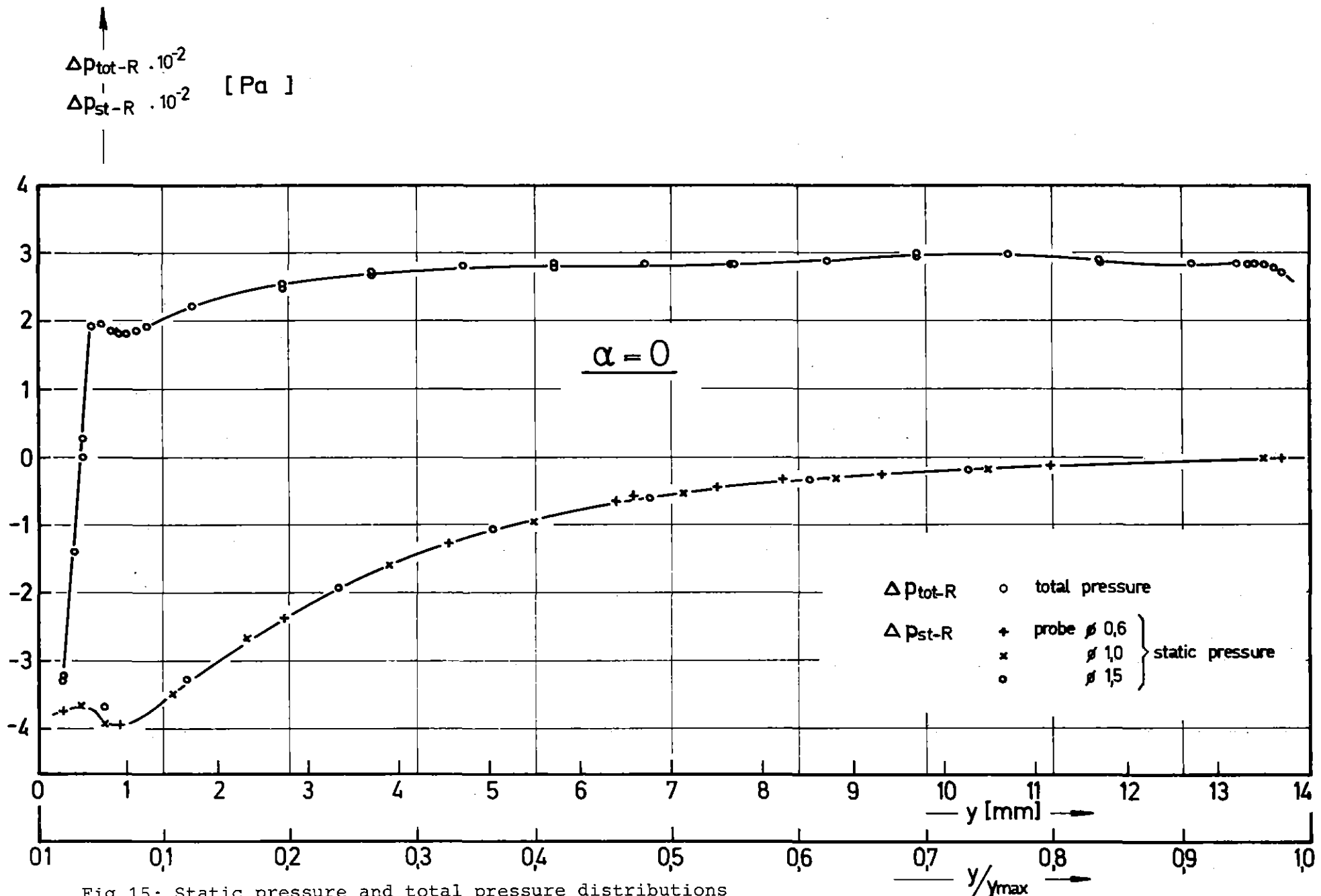


Fig.15: Static pressure and total pressure distributions

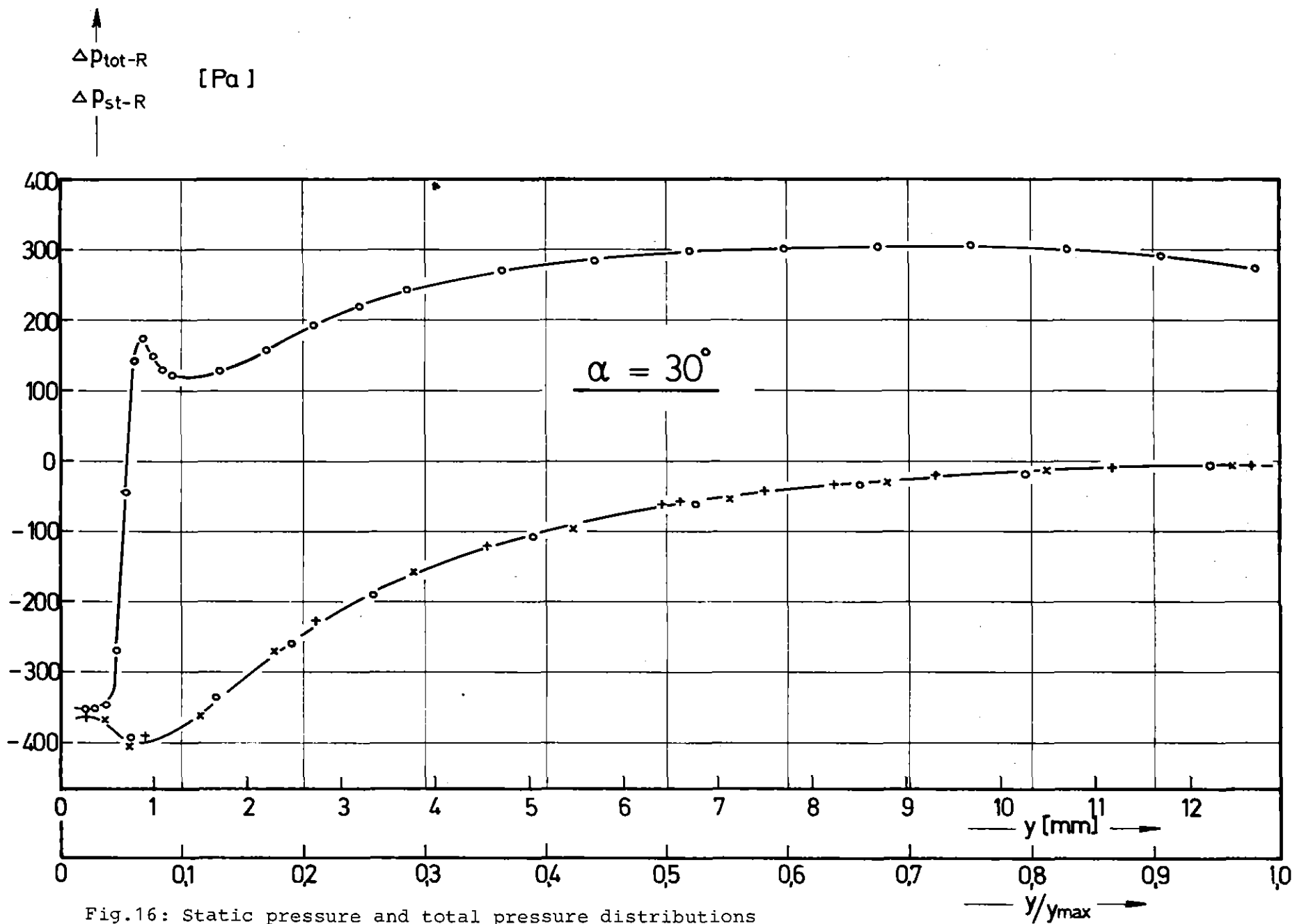


Fig.16: Static pressure and total pressure distributions

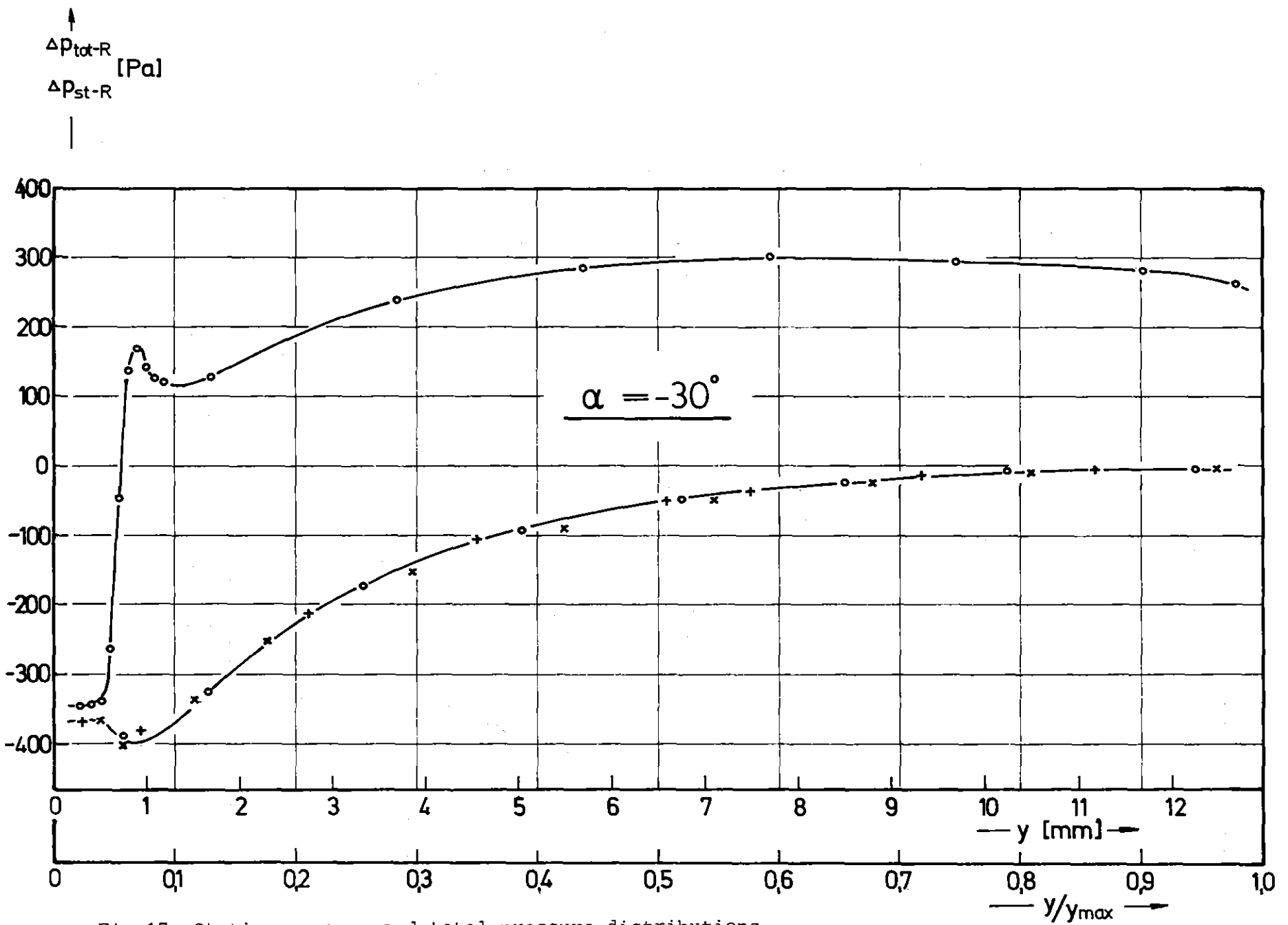


Fig.17: Static pressure and total pressure distributions

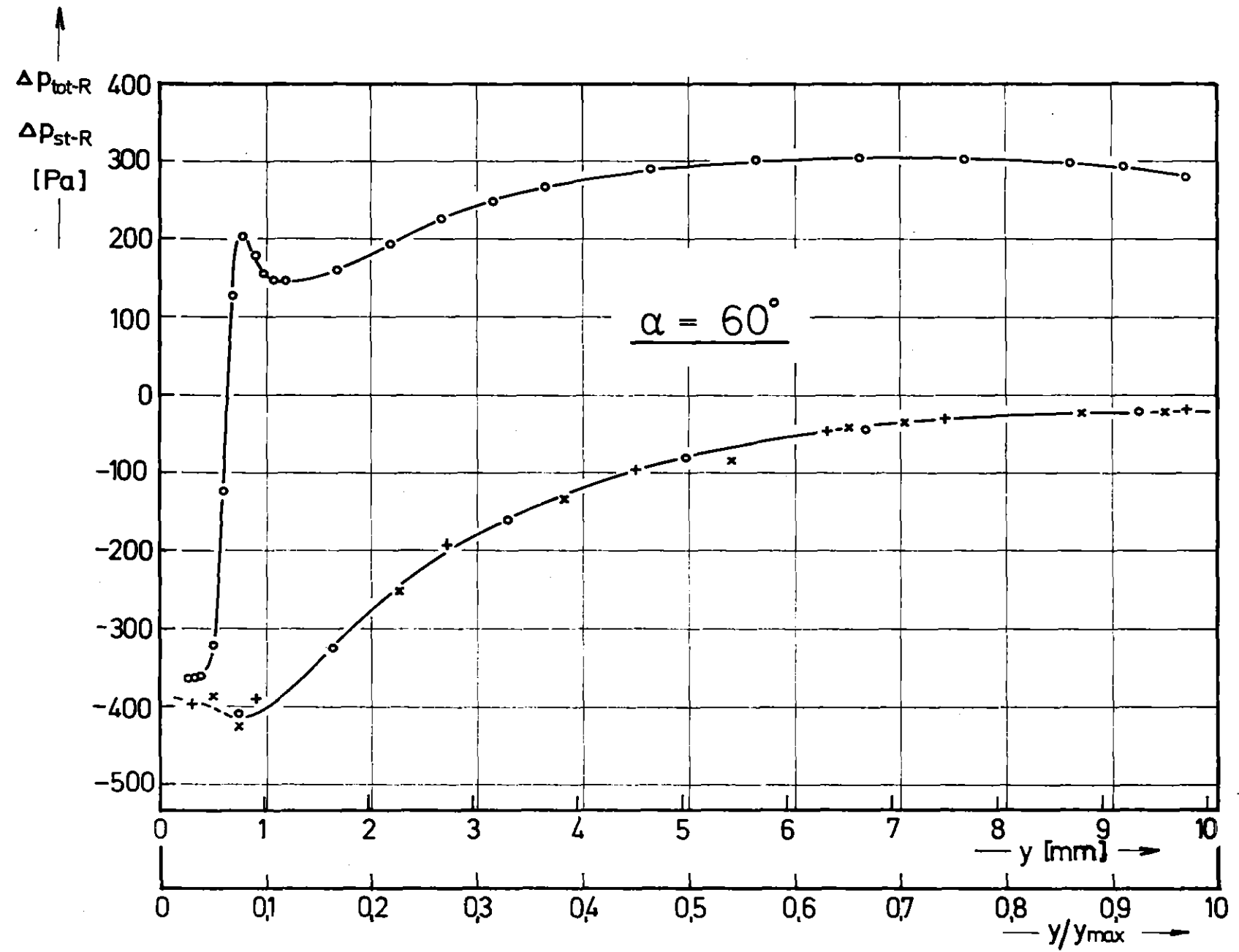


Fig.18: Static pressure and total pressure distributions

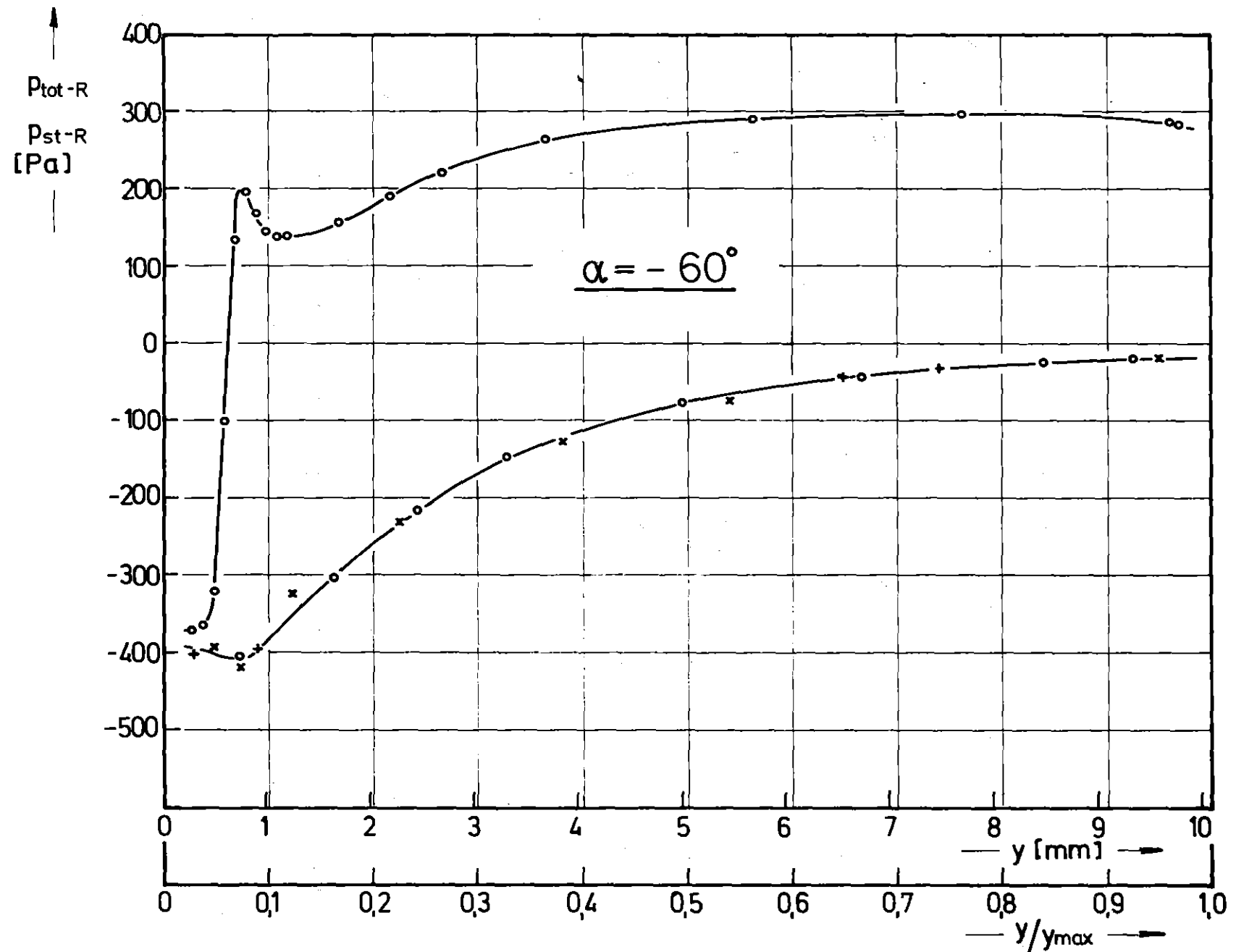


Fig.19: Static pressure and total pressure distributions

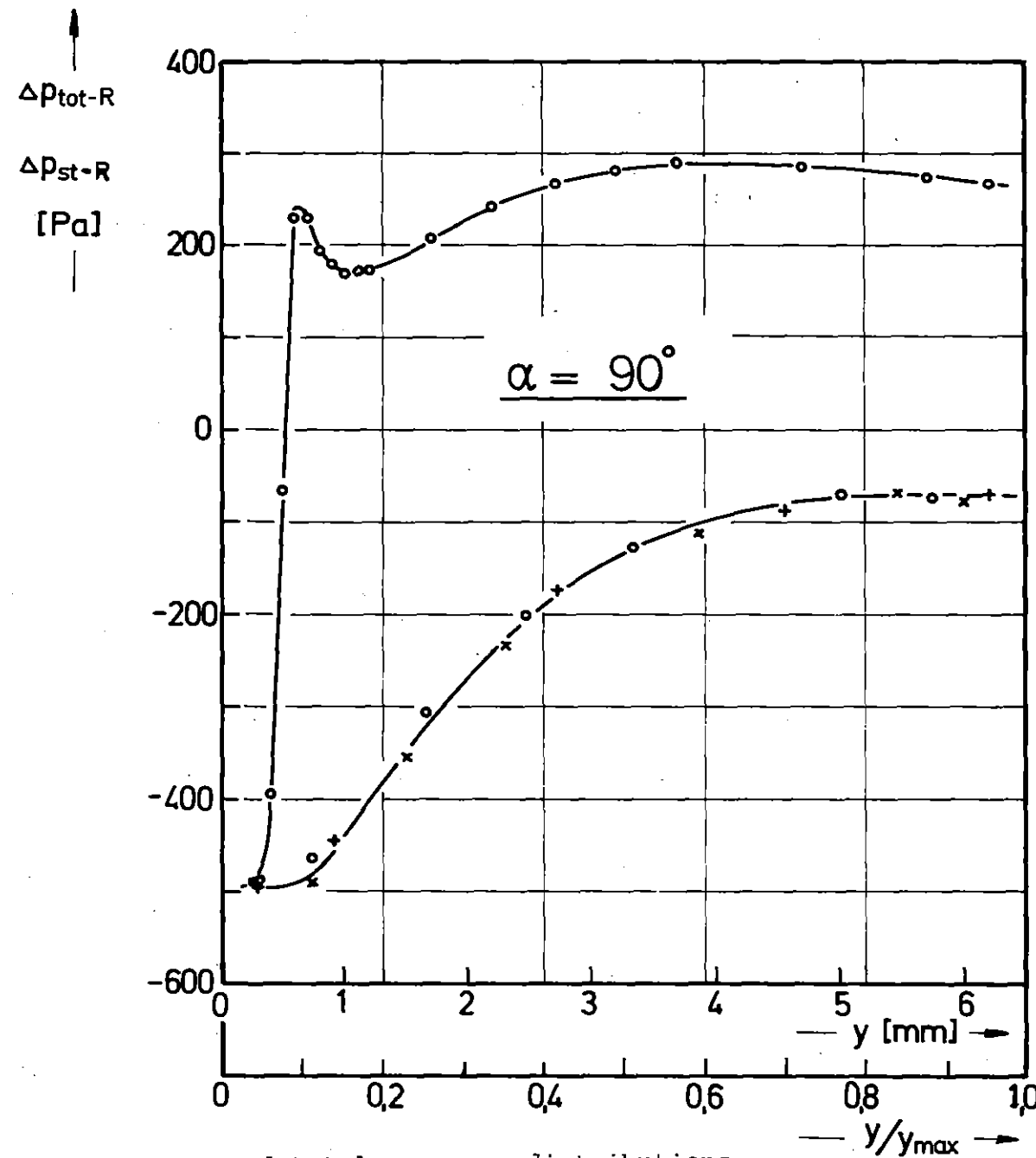


Fig.20: Static pressure and total pressure distributions

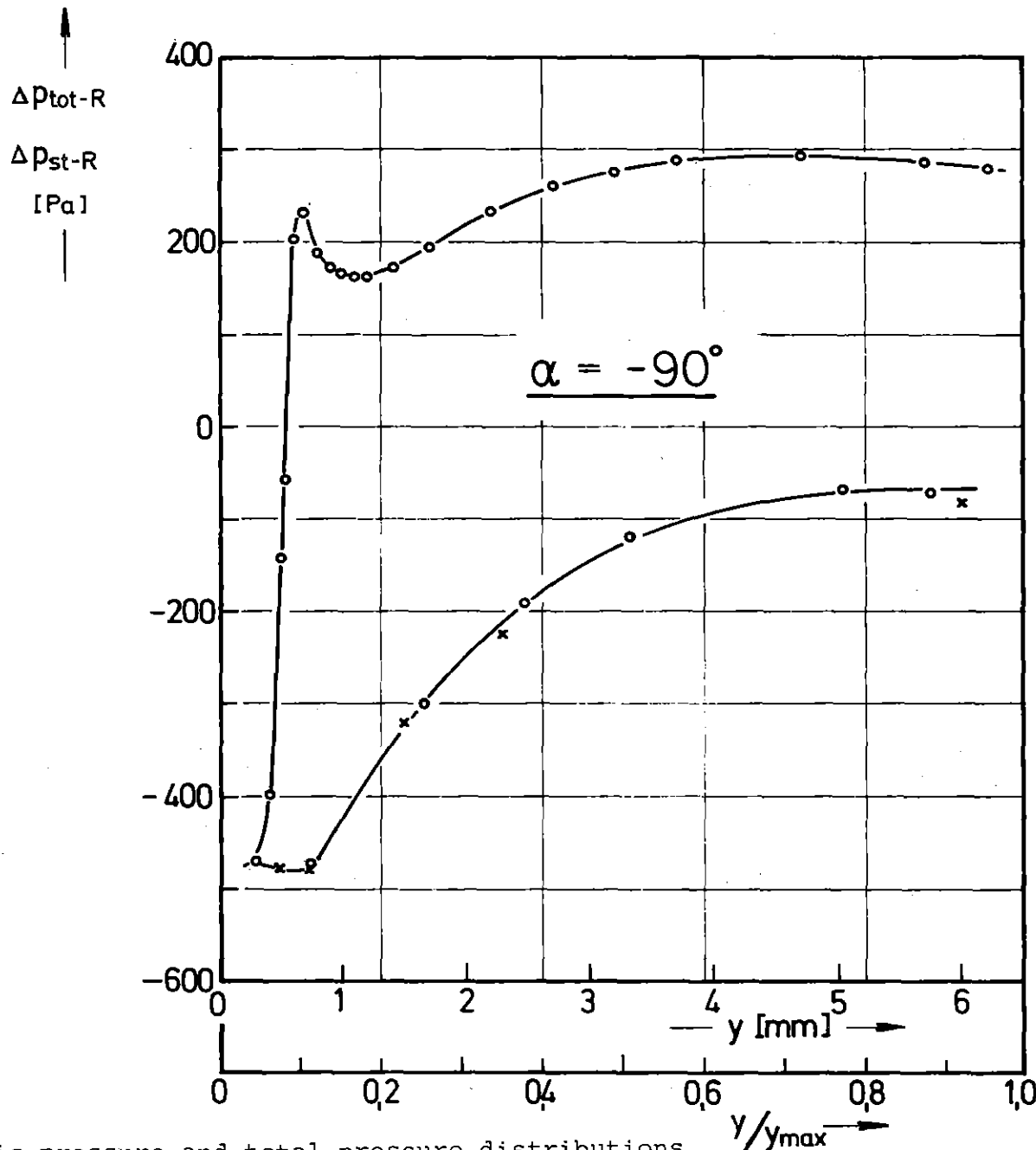


Fig.21: Static pressure and total pressure distributions

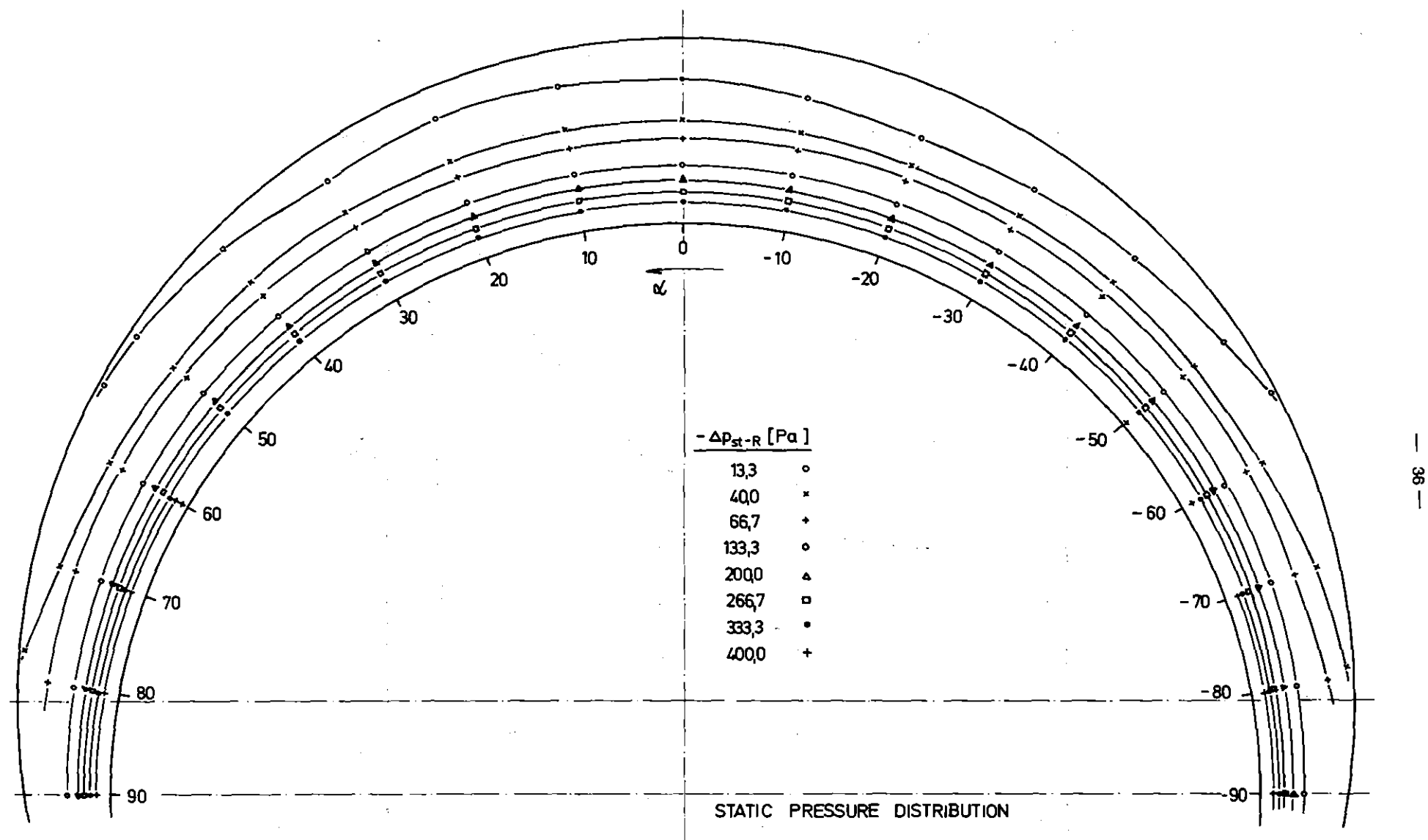


Fig.22: Static pressure distribution

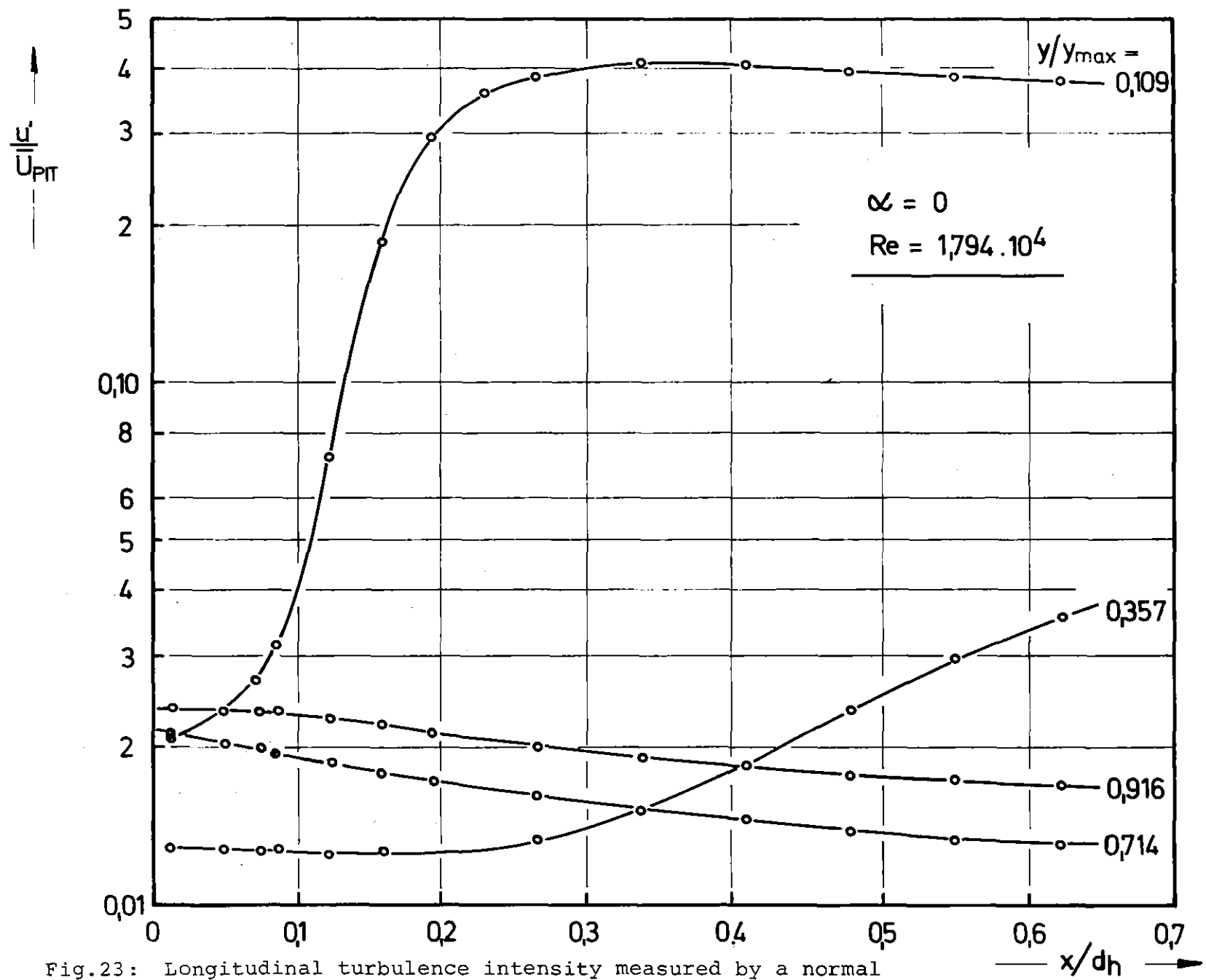


Fig. 23: Longitudinal turbulence intensity measured by a normal wire probe

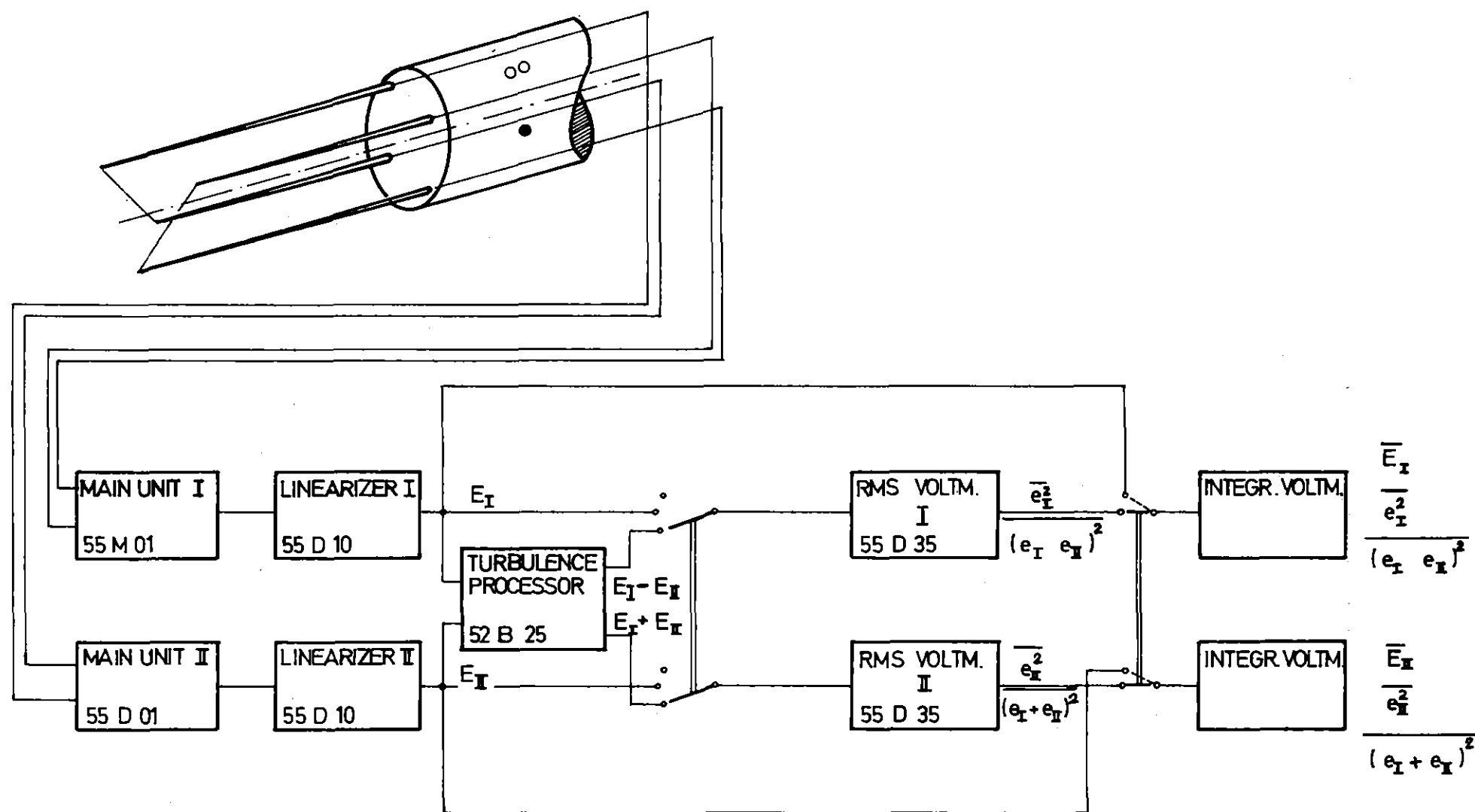


Fig.24: The measuring setup for x-wire measurements

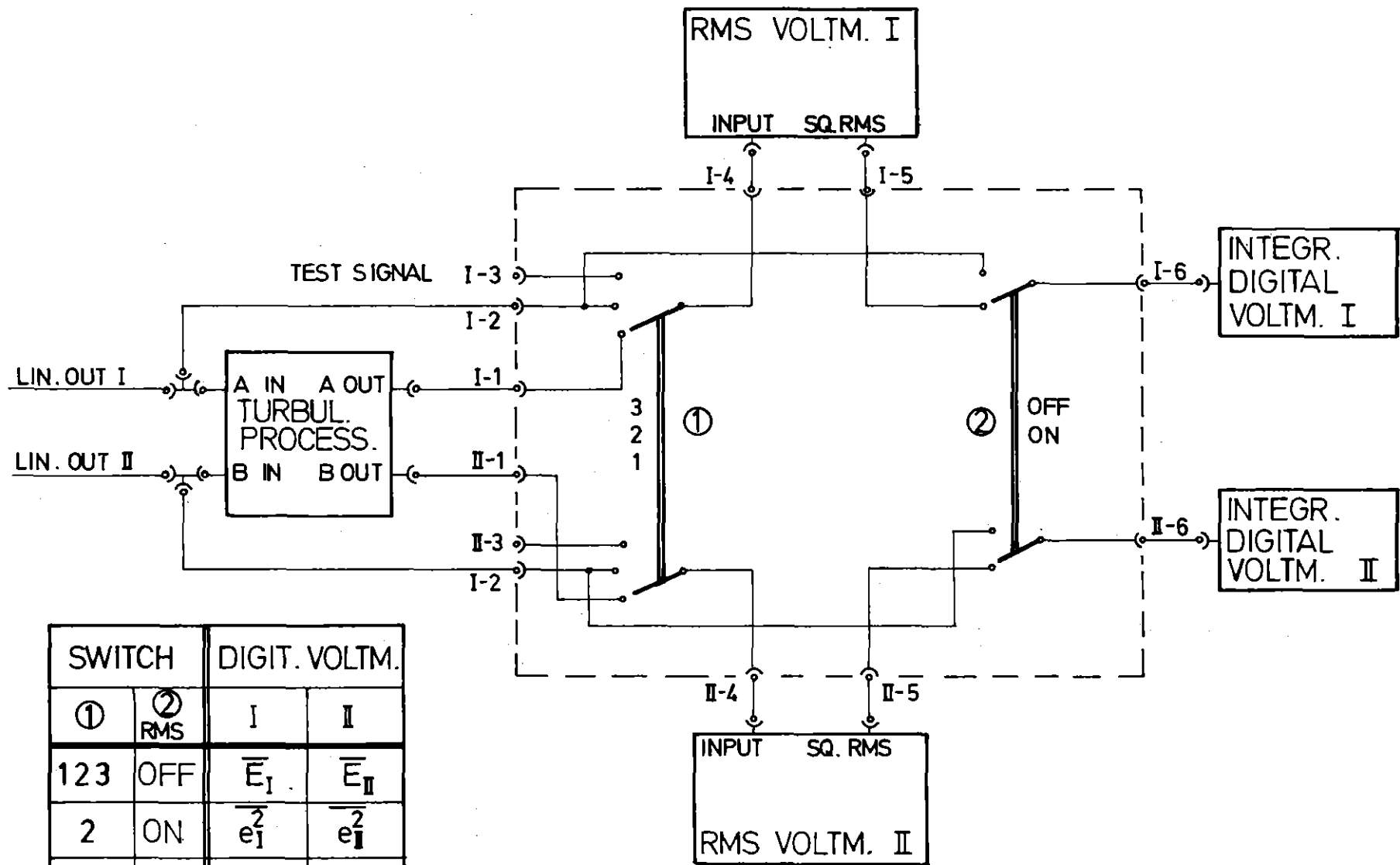


Fig. 25: The measuring setup for x-wire measurements

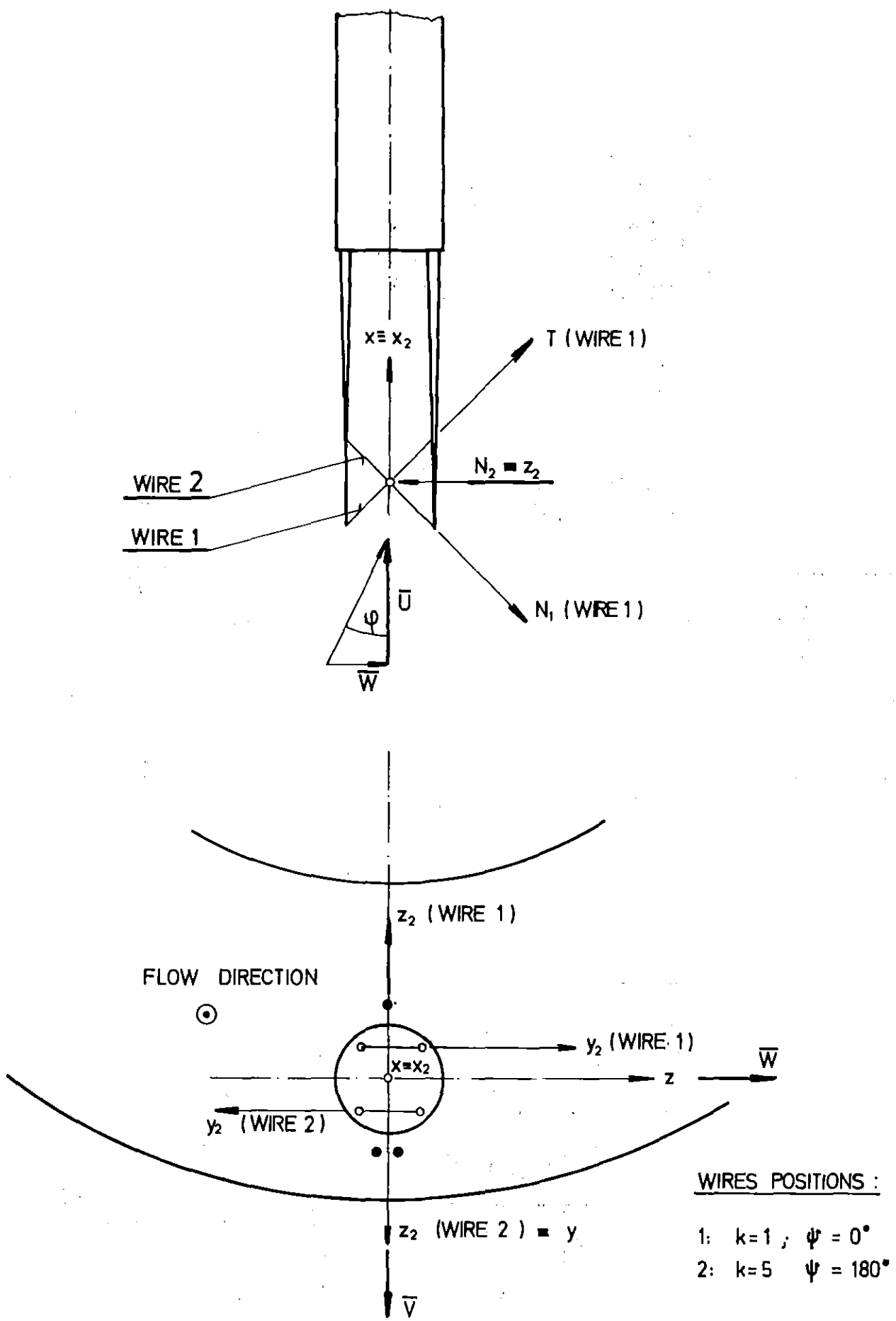


Fig. 26: Scheme of the coordinate systems

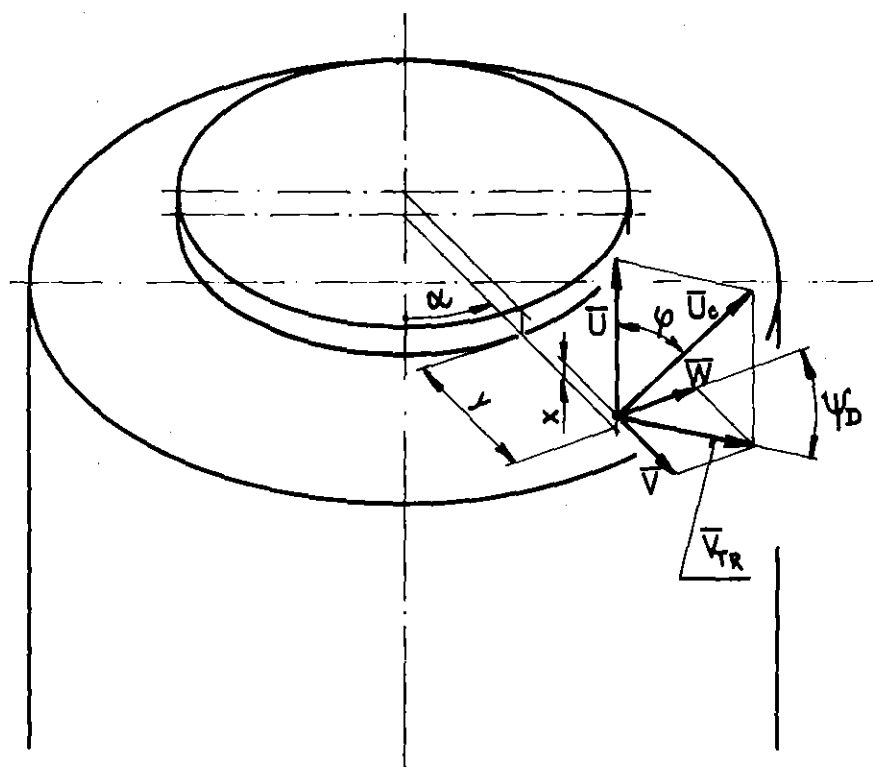
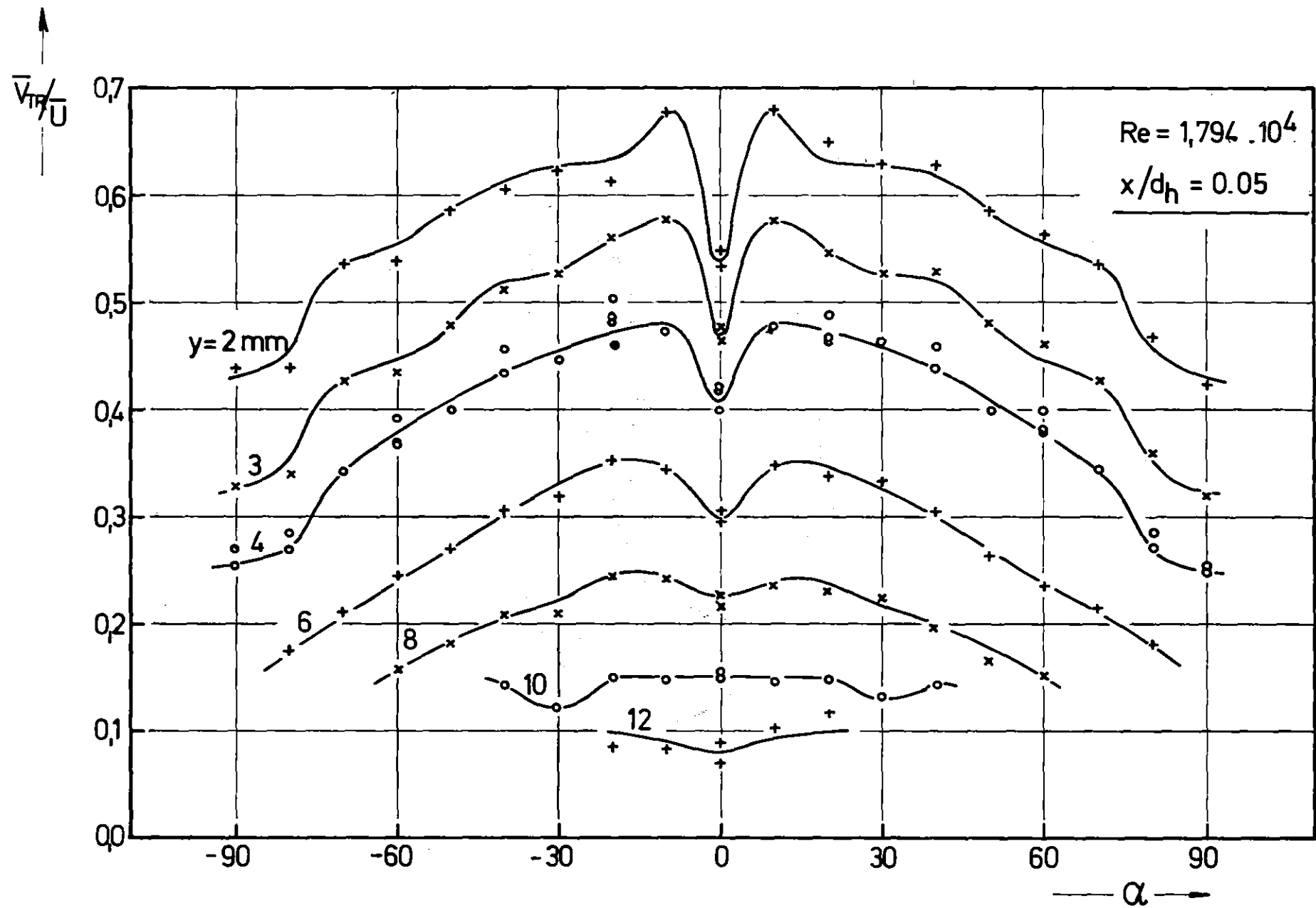


Fig.27: Scheme of the coordinate systems



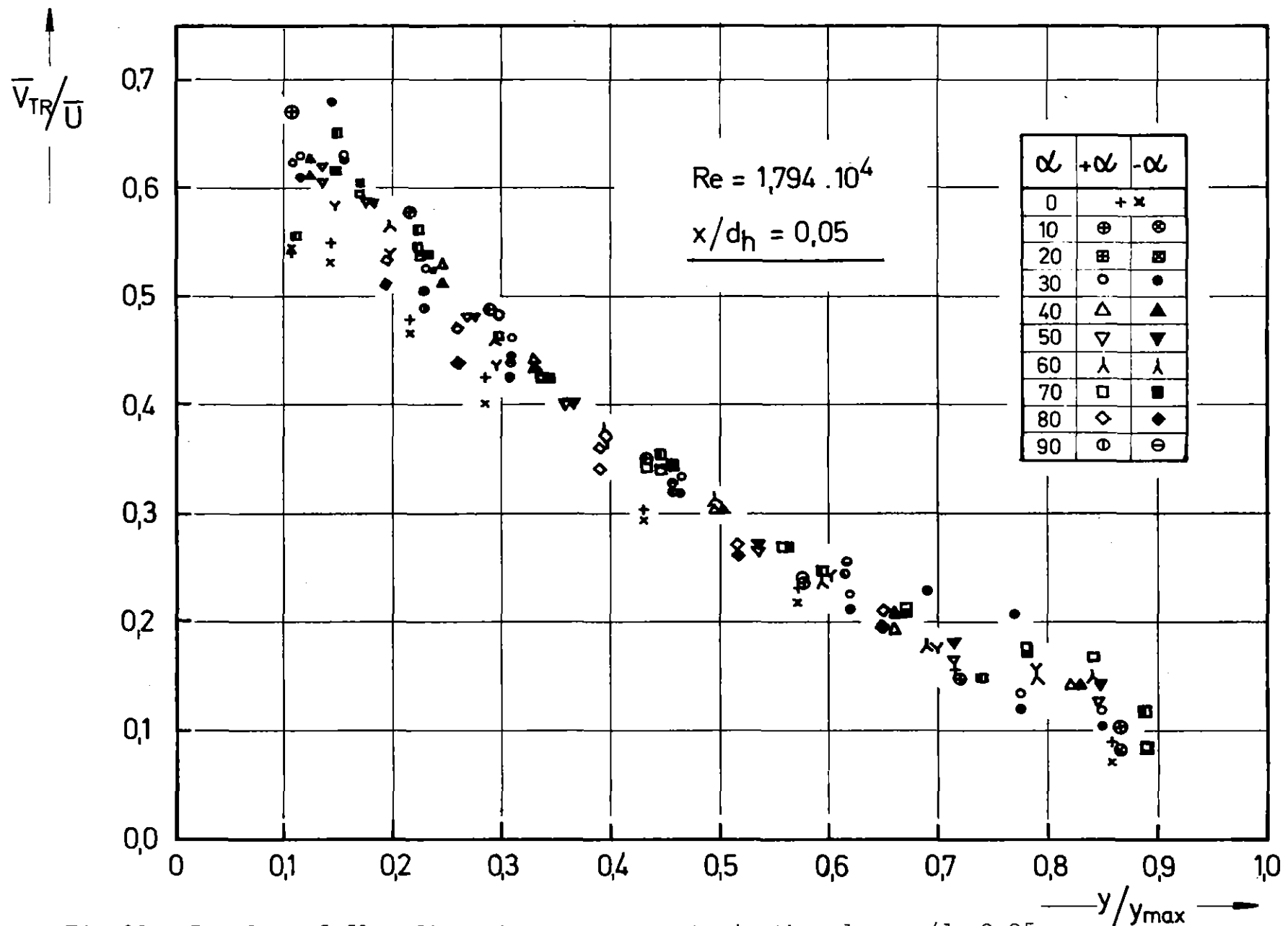


Fig. 29: Results of flow direction measurements in the plane $x/d_h=0,05$

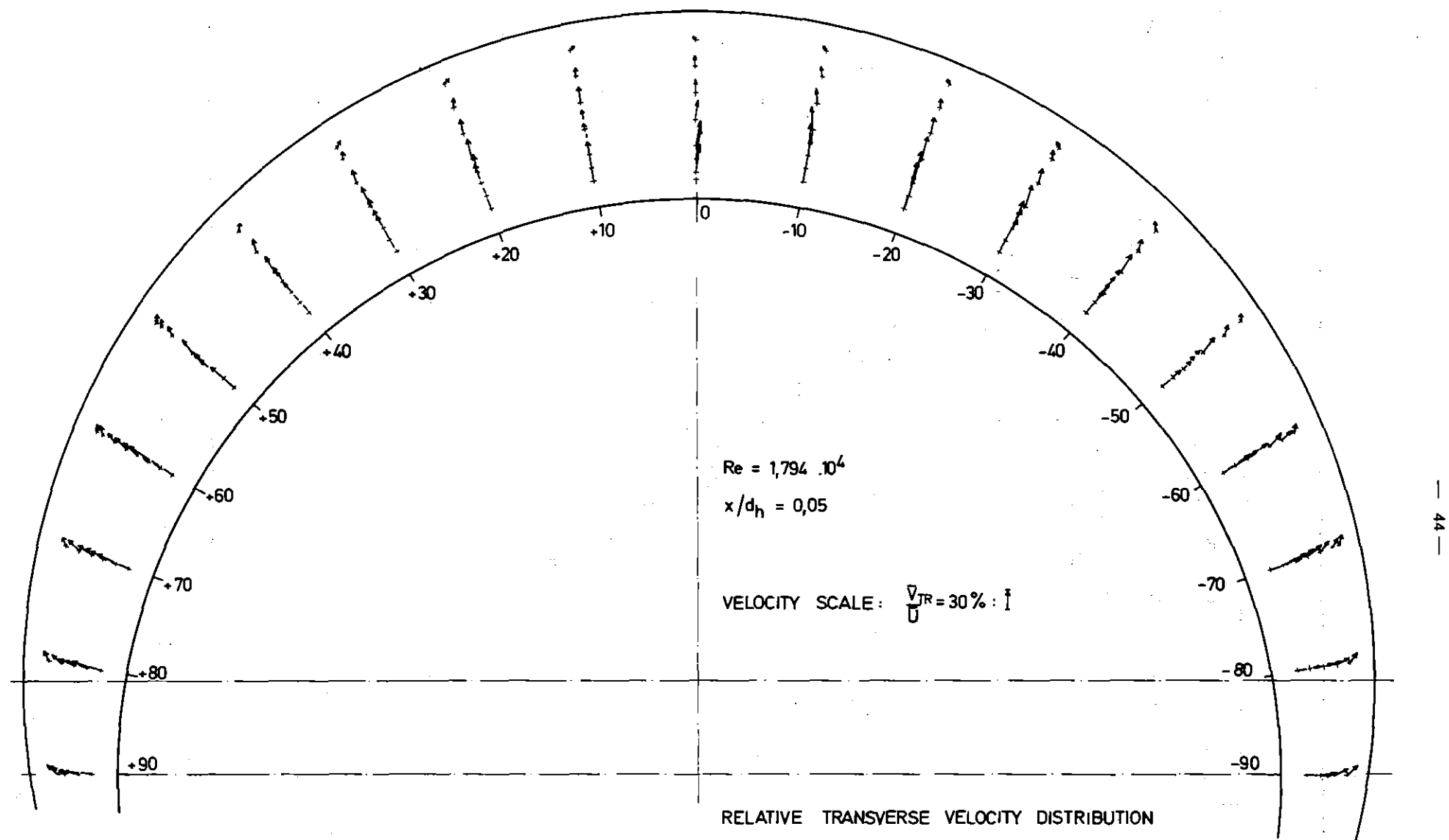


Fig.30: Results of flow direction measurements in the plane $x/d_h = 0,05$

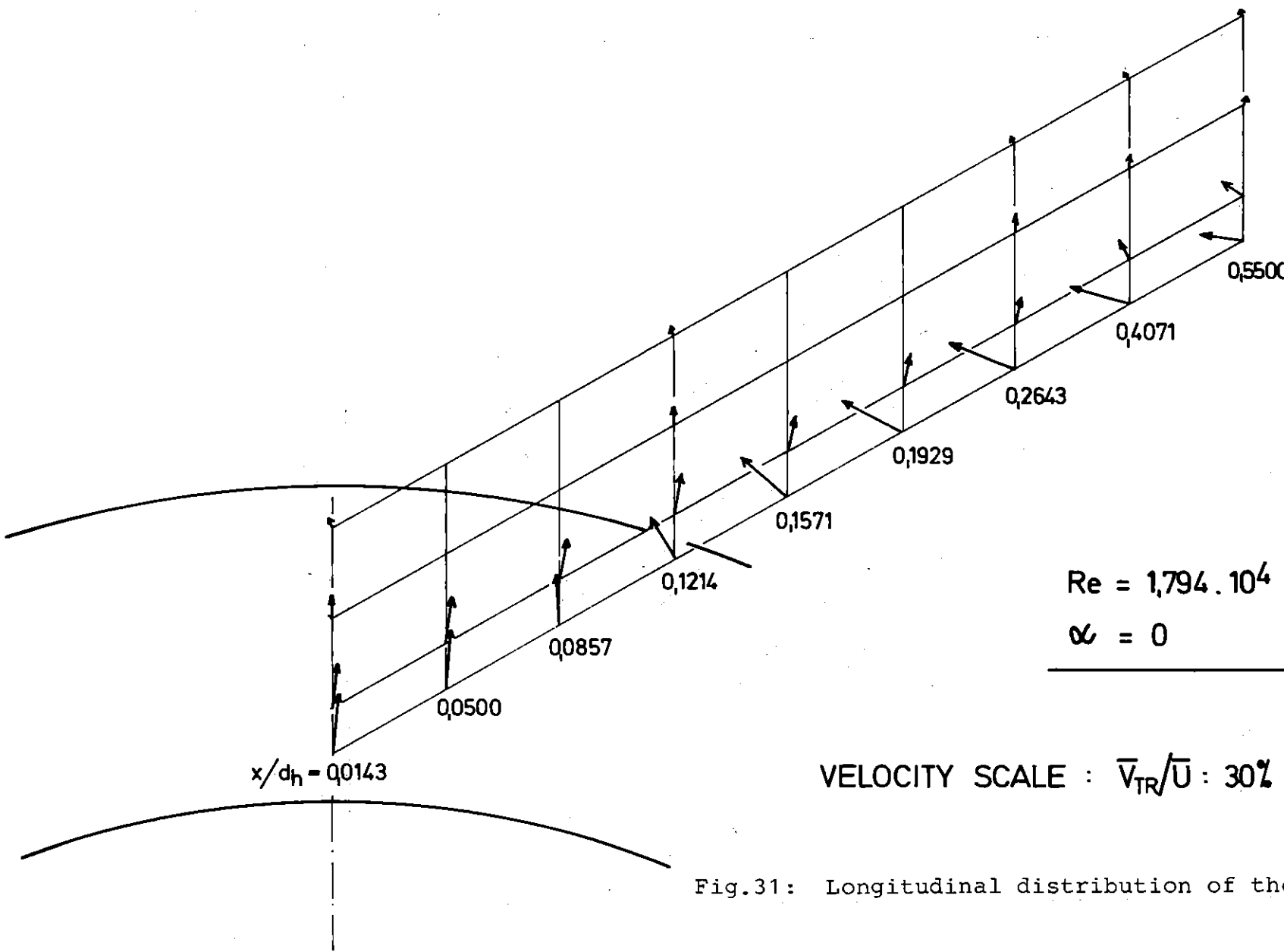


Fig.31: Longitudinal distribution of the flow direction

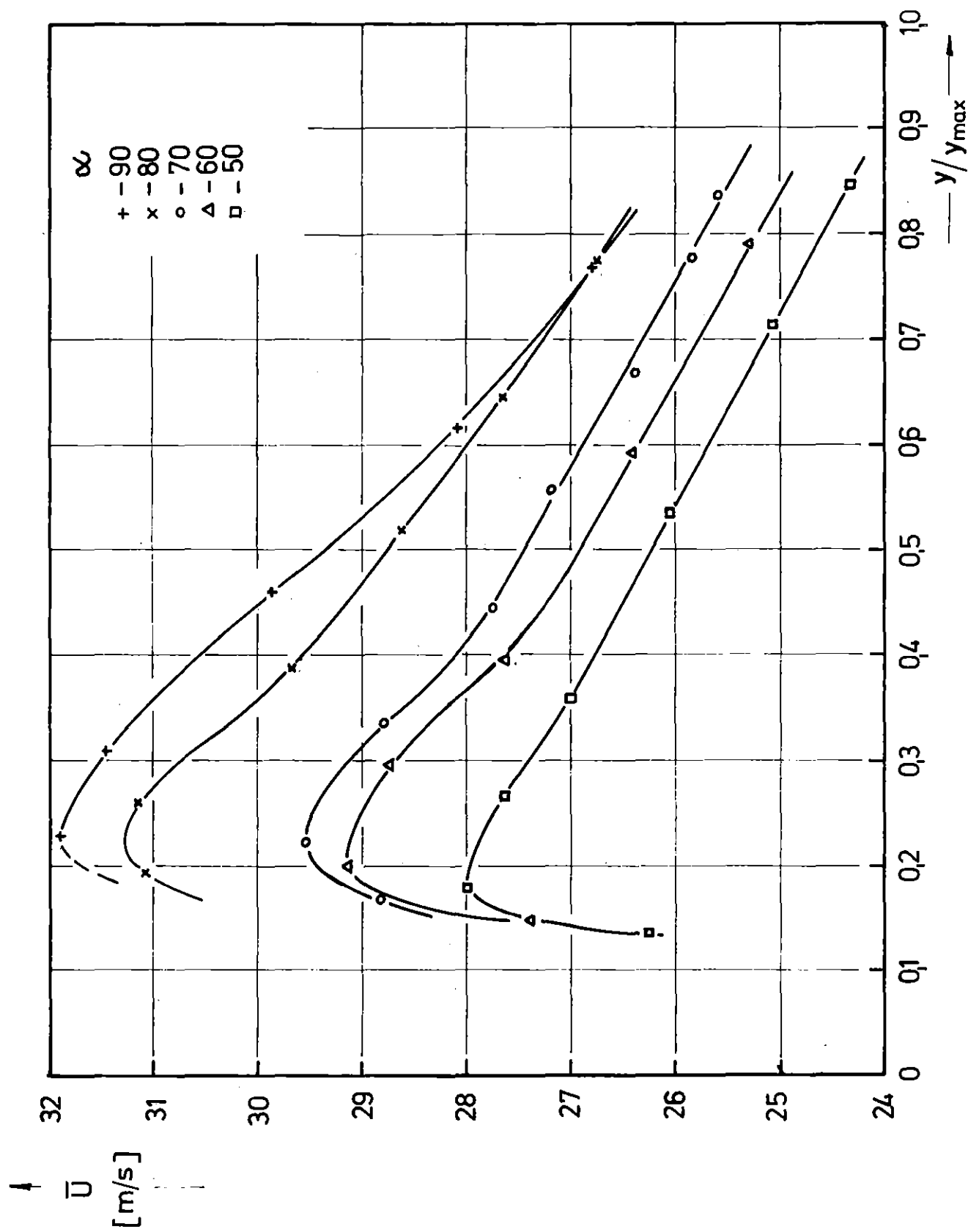


Fig. 32: Axial velocity distribution in the plane $x/d_h = 0,05$.

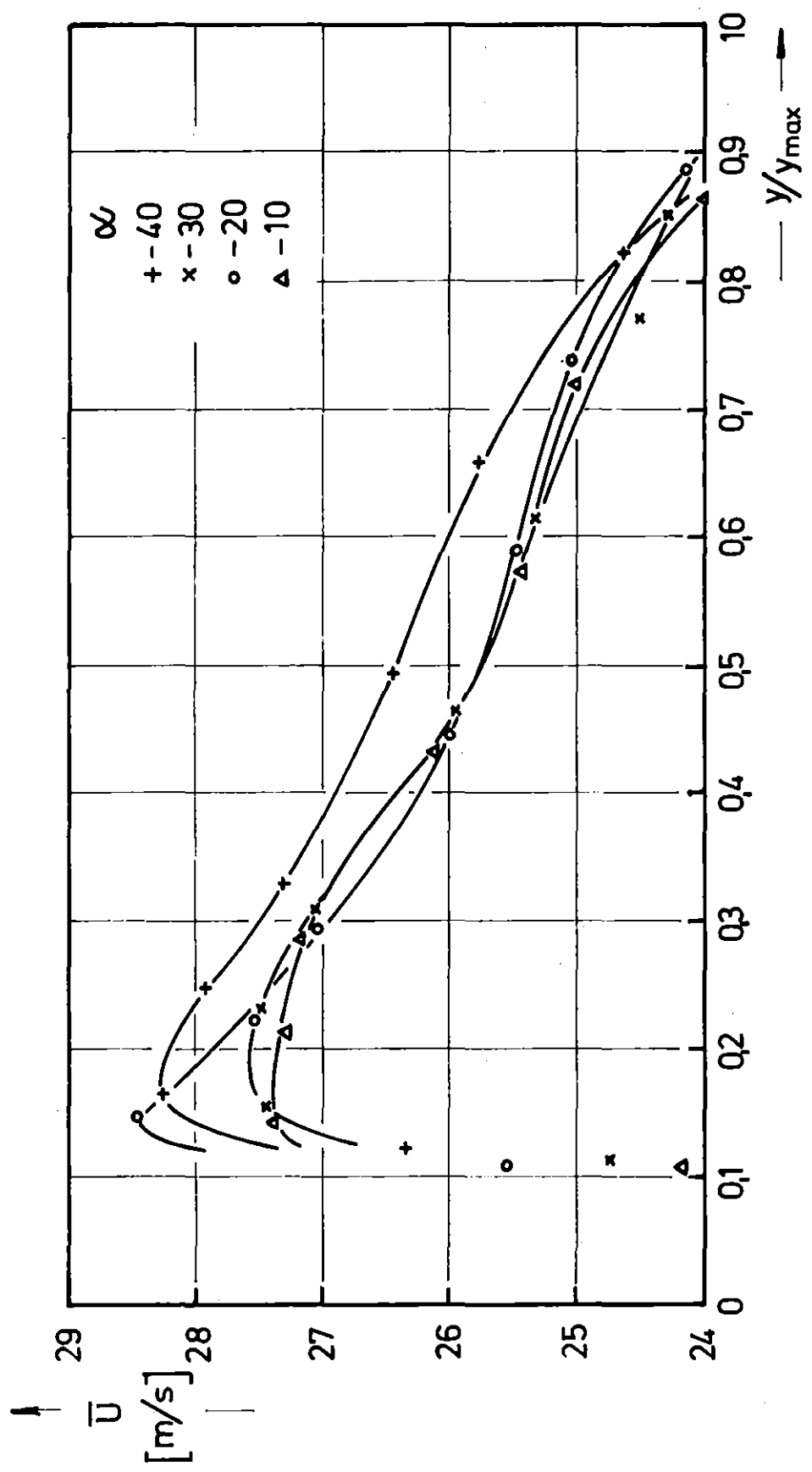


Fig. 33: Axial velocity distribution in the plane $x/d_h = 0,05$.

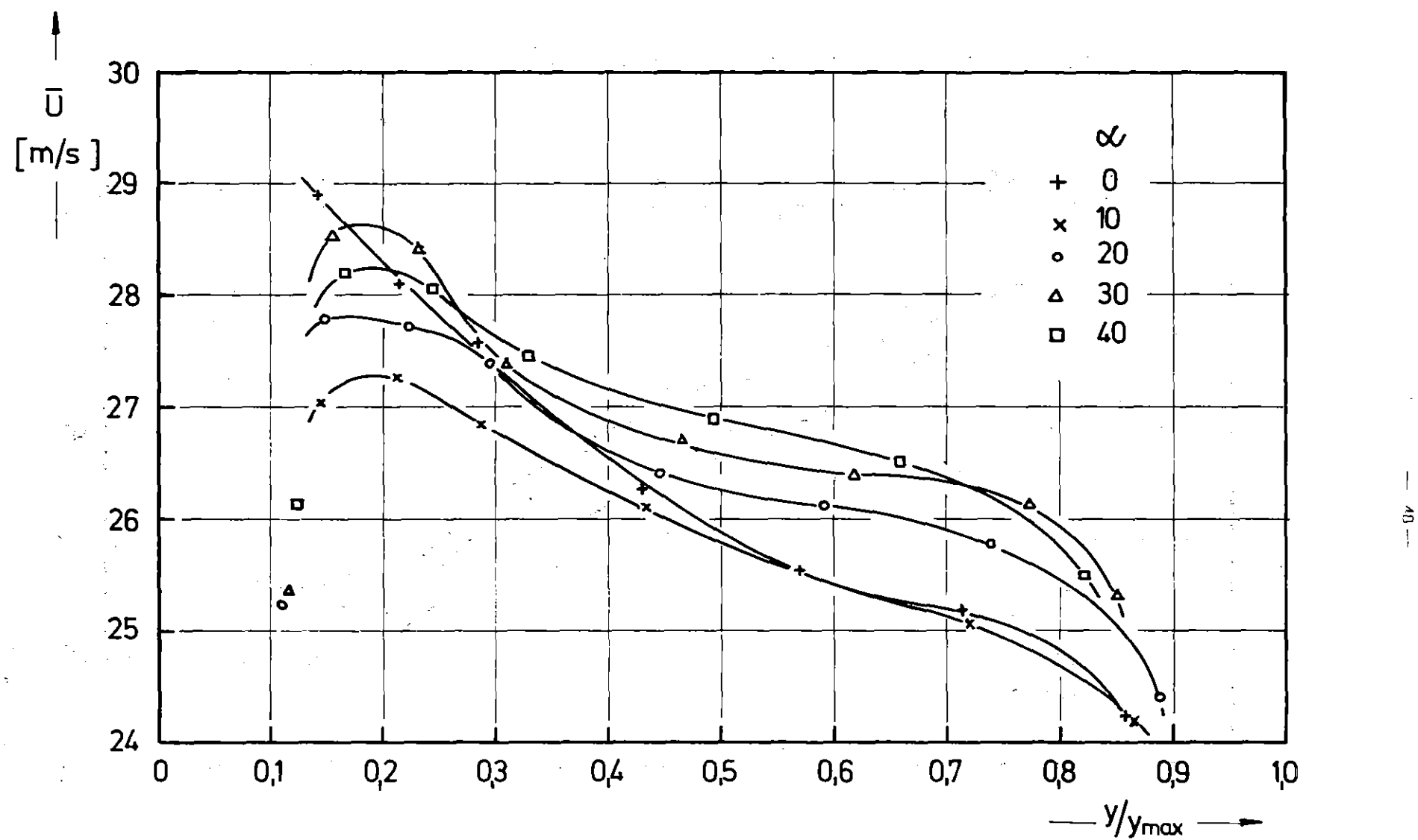


Fig.34: Axial velocity distribution in the plane $x/d_h=0,05$.

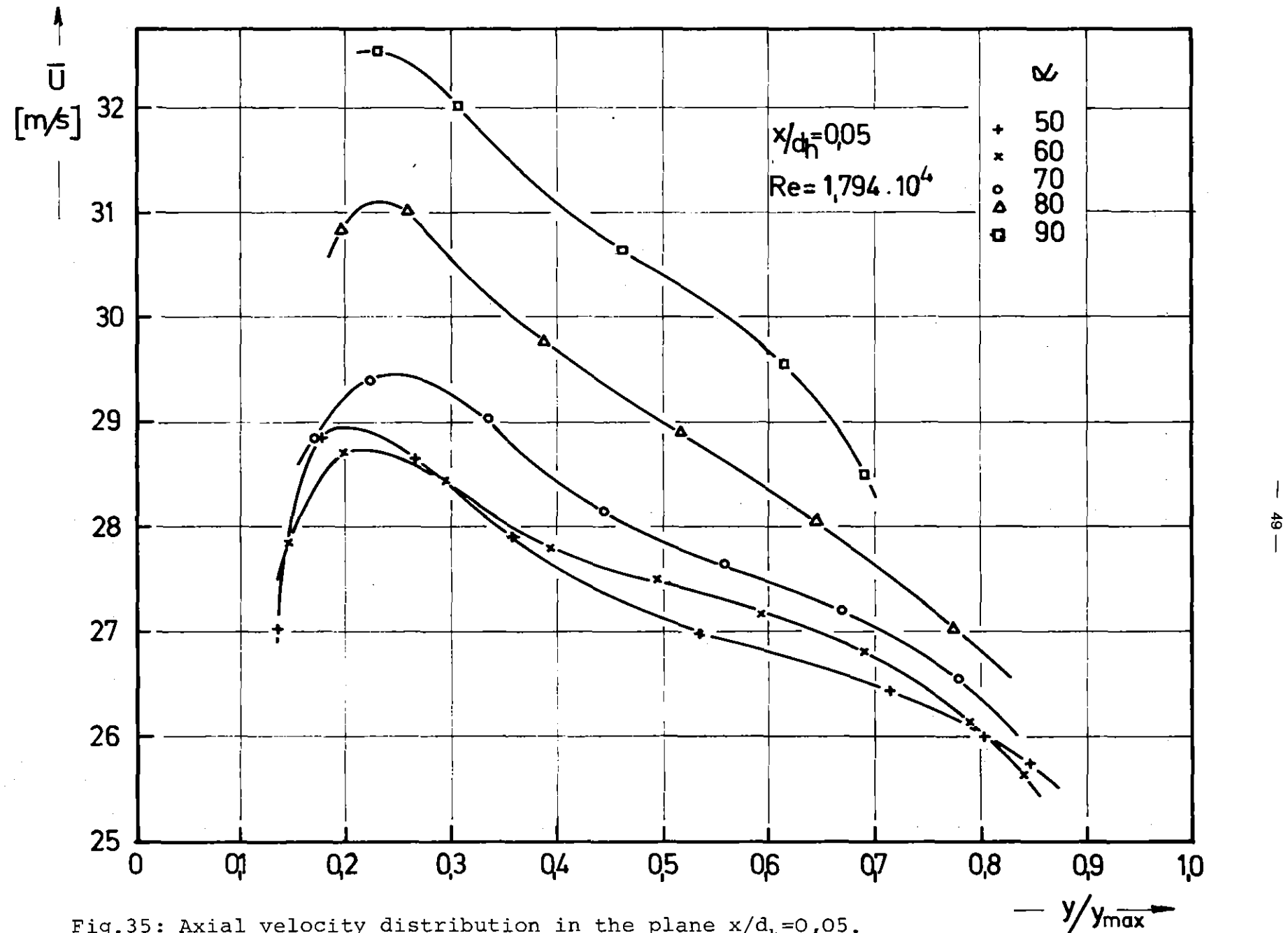


Fig. 35: Axial velocity distribution in the plane $x/d_h = 0,05$.

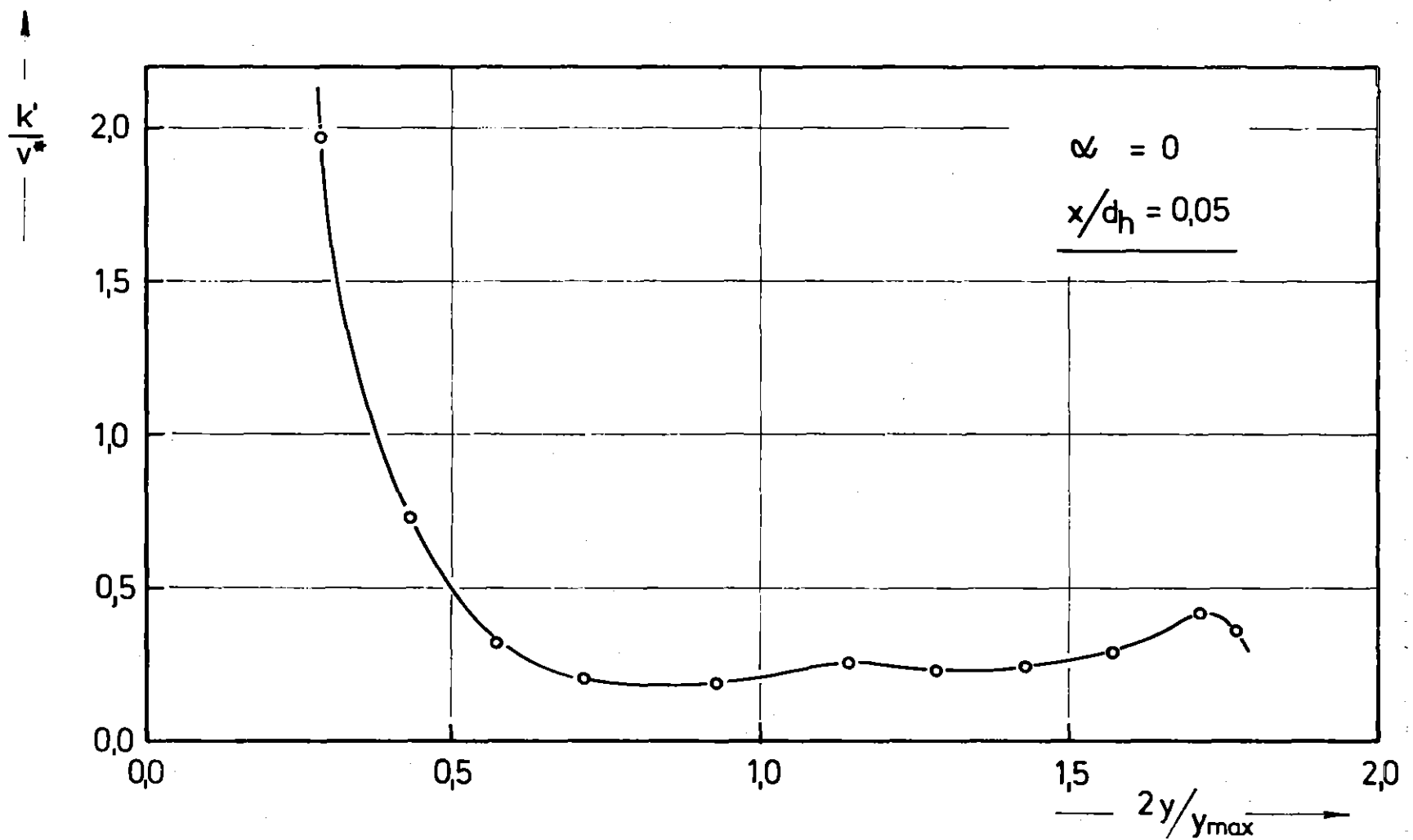


Fig.36: Results of fluctuation measurements ($x/d_h = 0,05$; $\alpha = 0$)

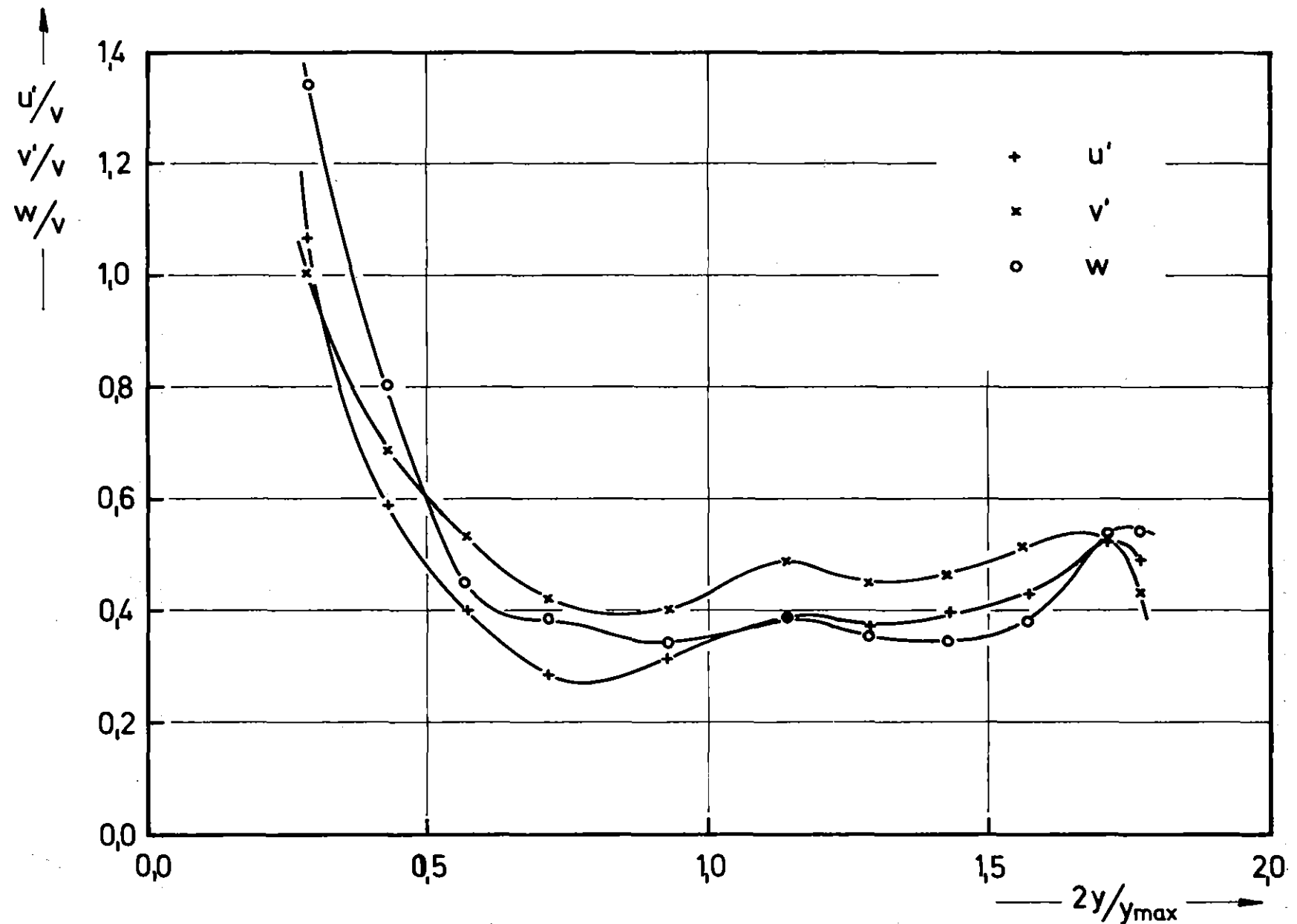


Fig.37: Results of fluctuation measurements ($x/d_h=0,05$; $\alpha=0$)

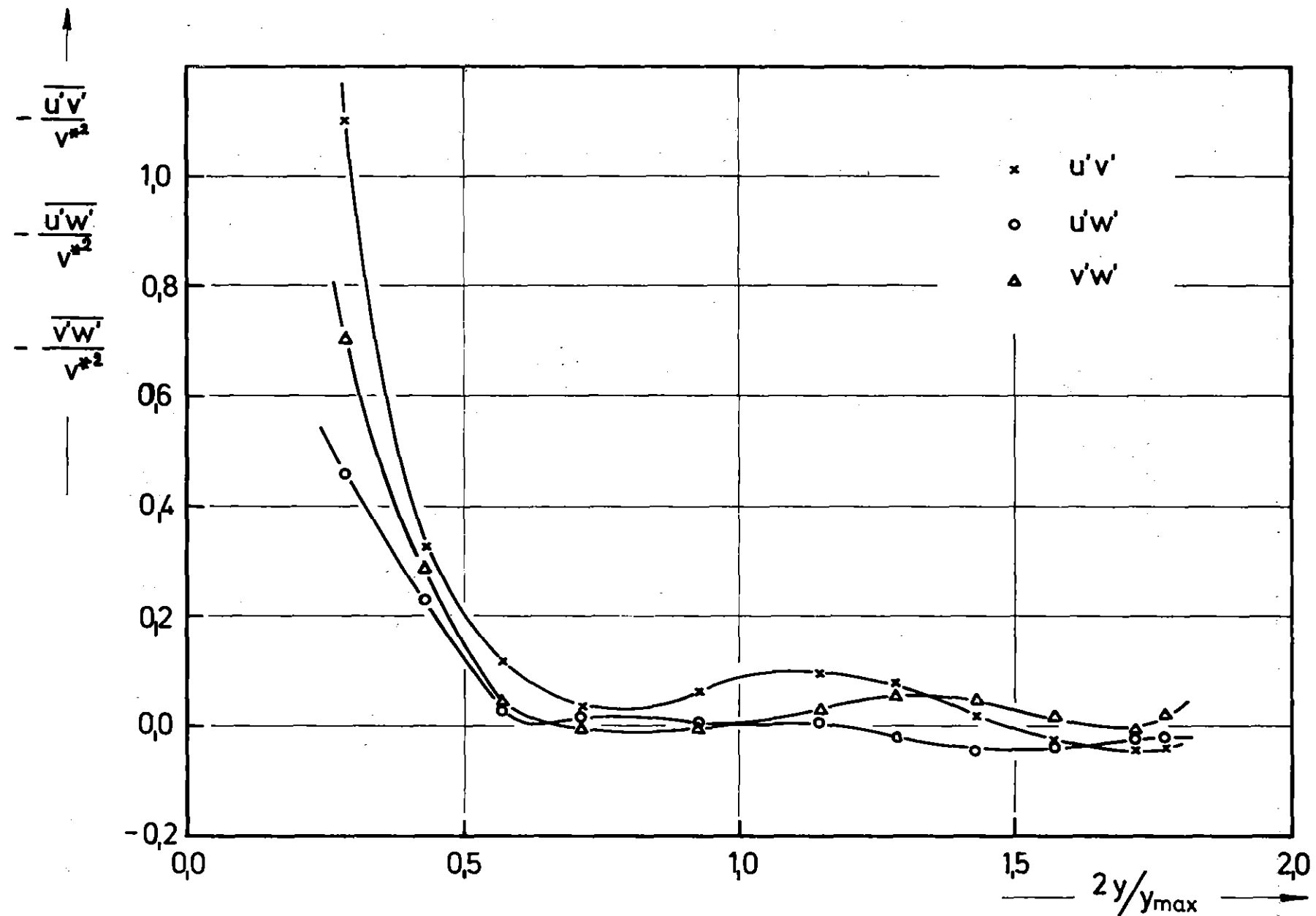


Fig. 38: Results of fluctuation measurements ($x/d_h = 0,05$; $\alpha = 0$)

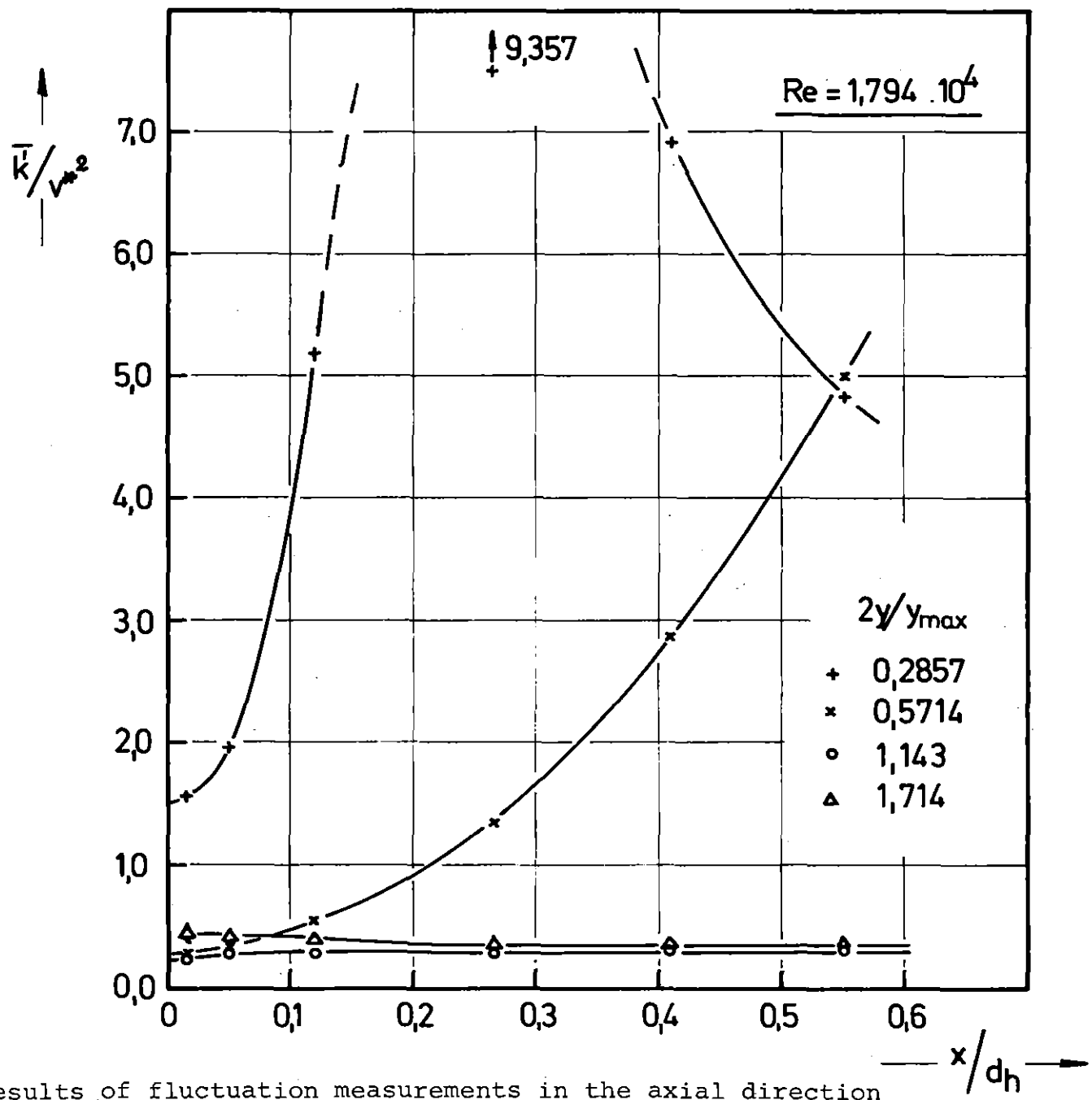


Fig. 39: Results of fluctuation measurements in the axial direction

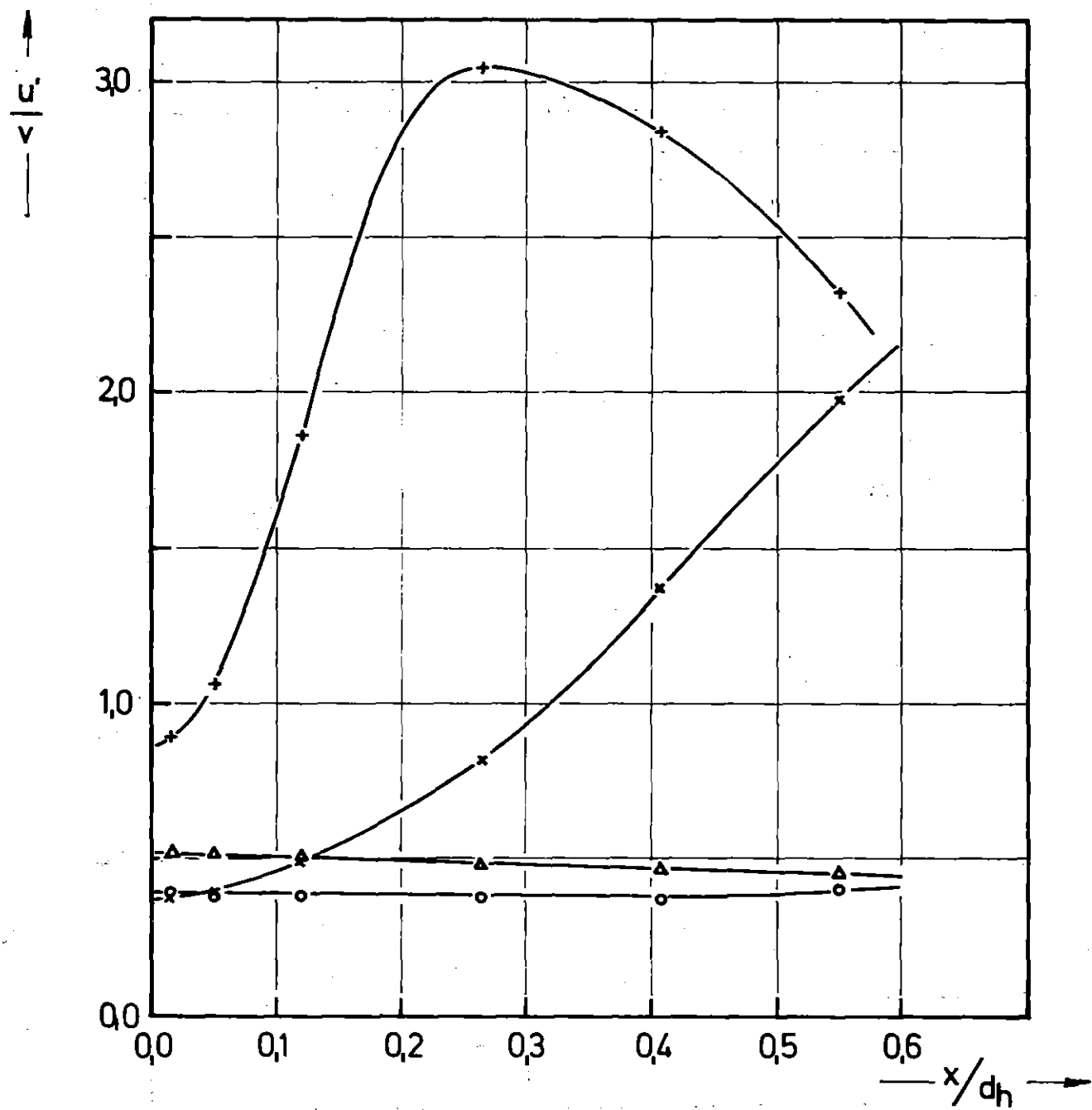


Fig.40: Results of fluctuation measurements in the axial direction

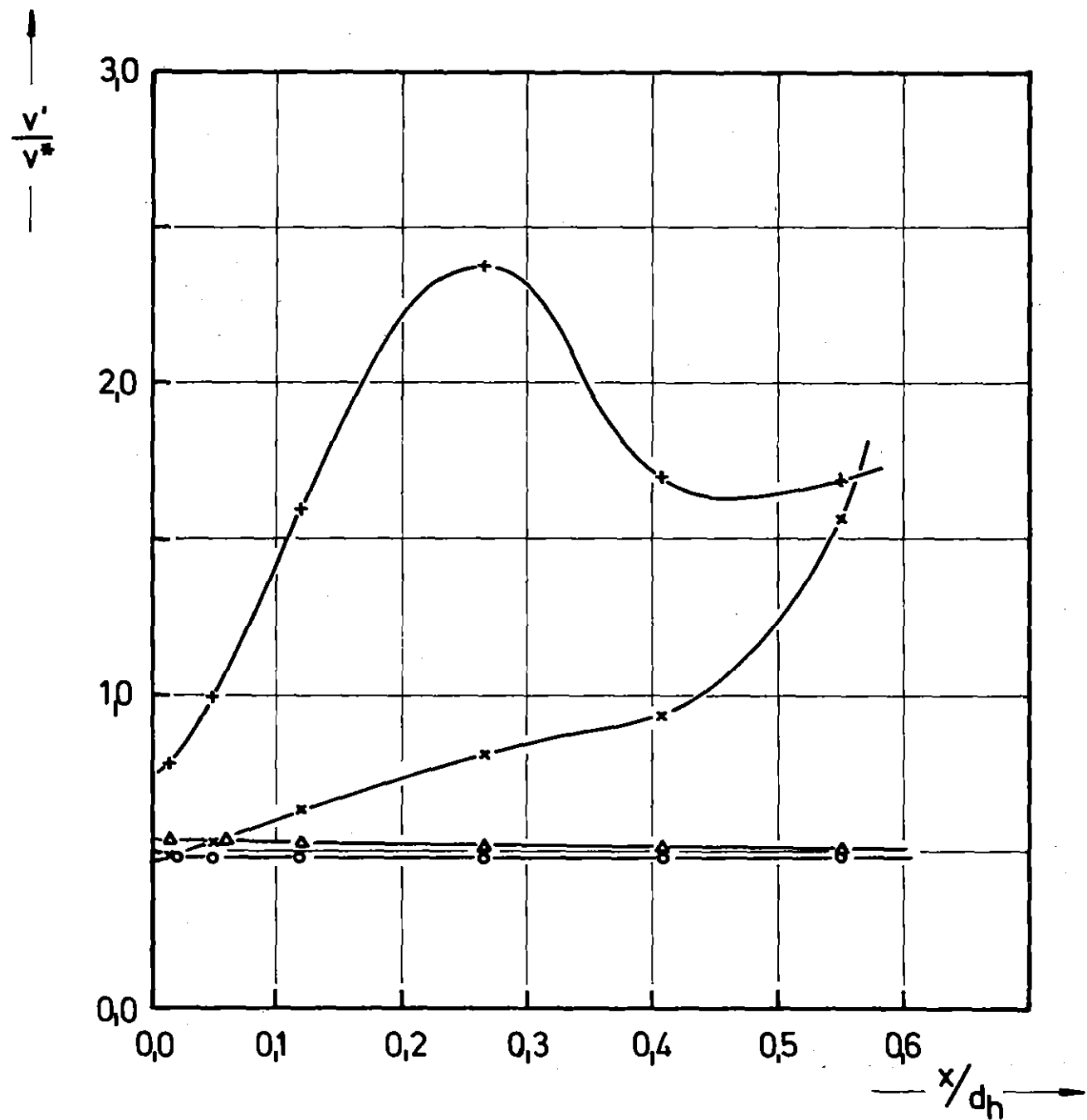


Fig. 41: Results of fluctuation measurements in the axial direction

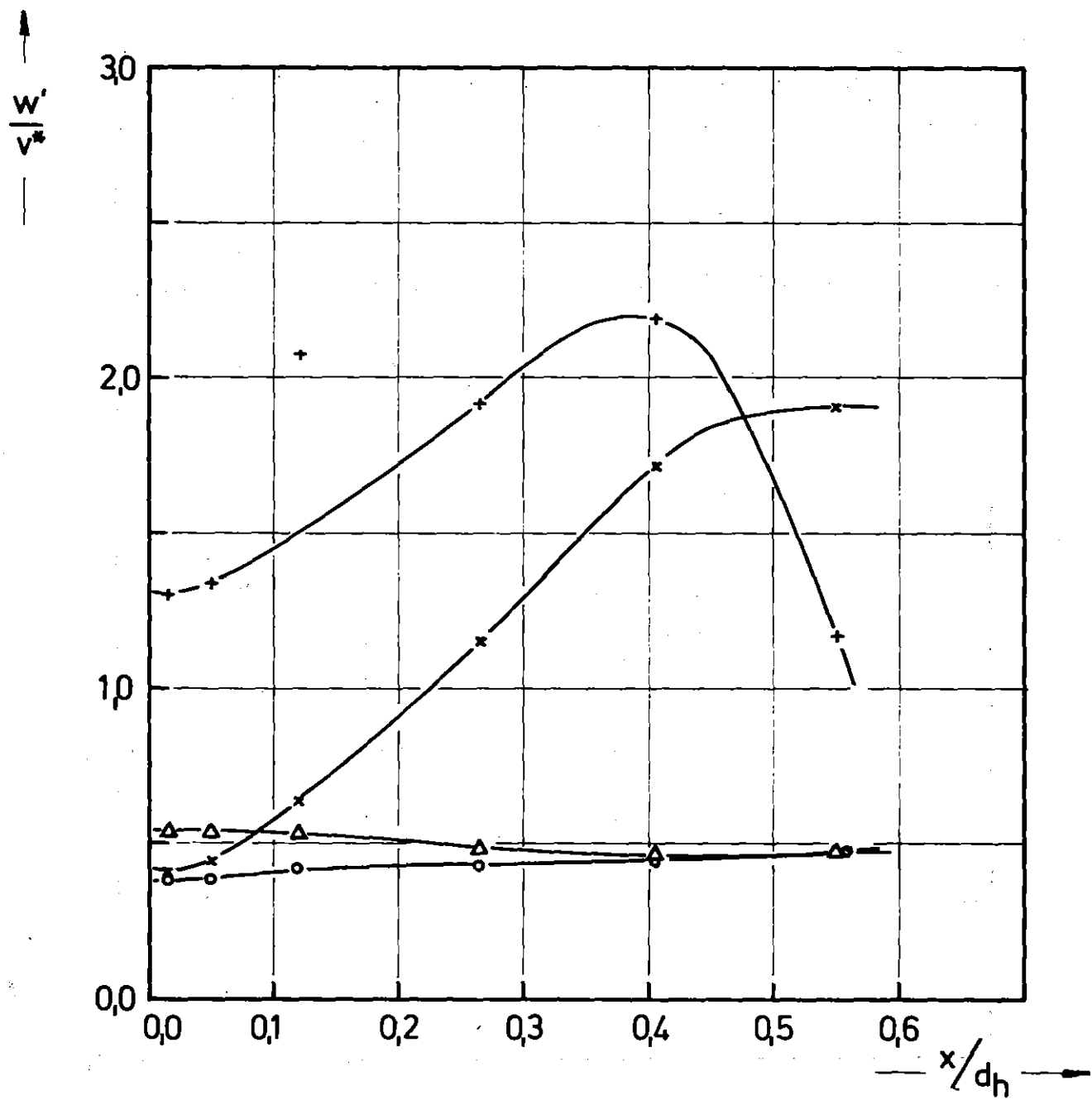


Fig. 42: Results of fluctuation measurements in the axial direction

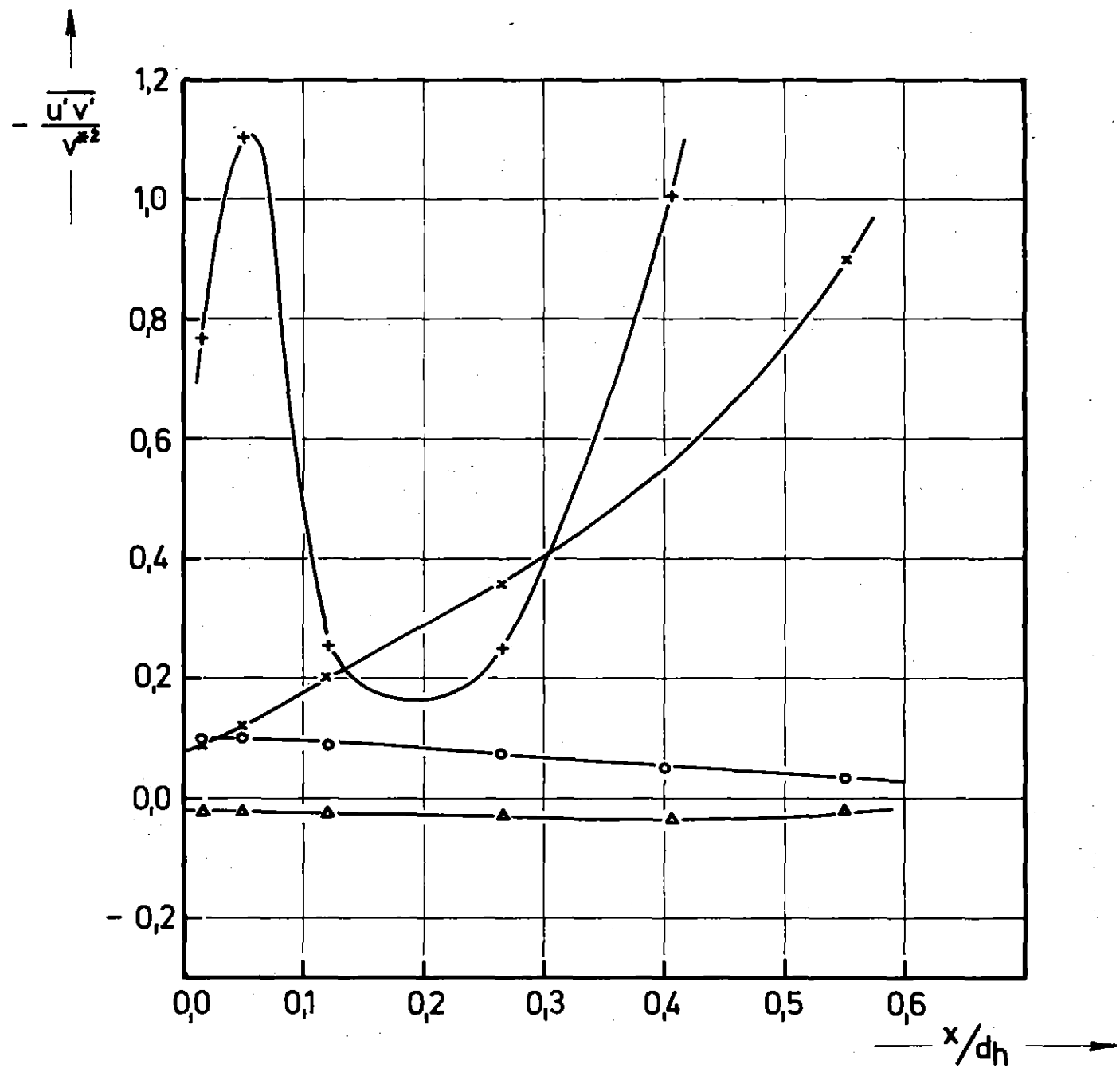


Fig. 43: Results of fluctuation measurements in the axial direction

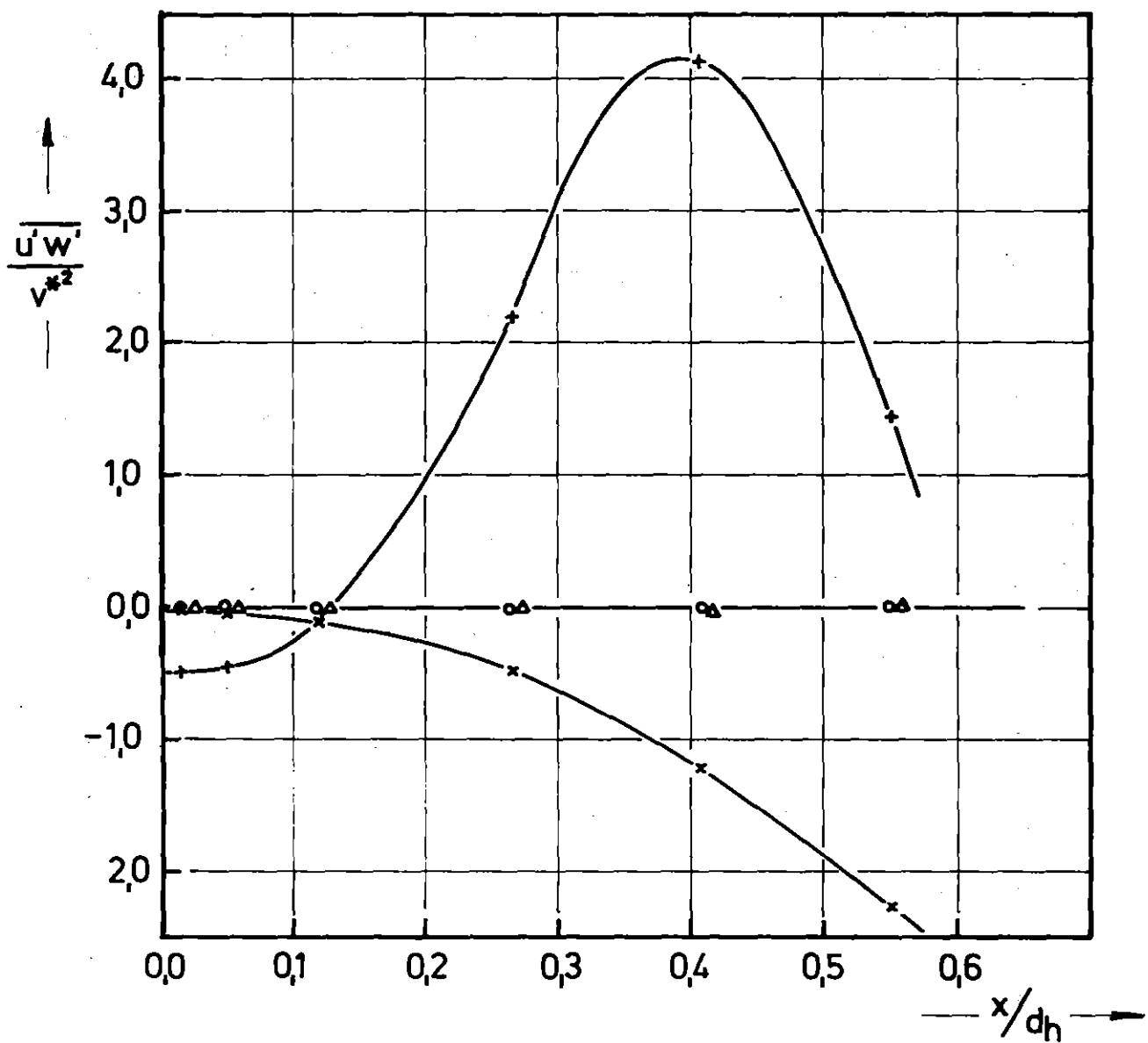
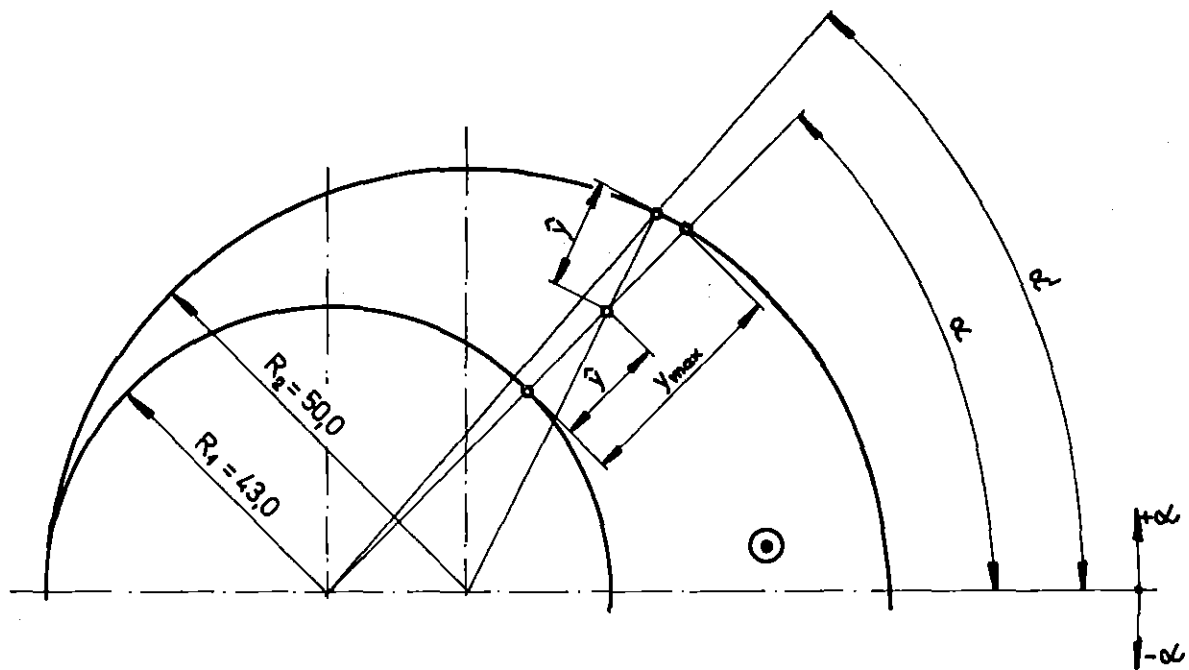


Fig. 44: Results of fluctuation measurements in the axial direction



α grad	α'	\hat{y} [mm]	y_{max}
0	0,00	7,00	14,00
10	10,20	6,94	13,88
20	20,38	6,76	13,52
30	30,53	6,46	12,94
40	40,65	6,07	12,16
50	50,71	5,59	11,21
60	60,74	5,05	10,13
70	70,71	4,46	8,96
80	80,65	3,85	7,74
90	90,56	3,24	6,51
100	100,46	2,64	5,31
110	110,35	2,08	4,17
120	120,24	1,56	3,13
130	130,15	1,10	2,31
140	140,08	0,71	1,44
150	150,04	0,41	0,82
160	160,01	0,18	0,36
170	170,00	0,05	0,09
180	180,00	0,00	0,00

Tab.1: Geometry of the channel

Tab.2: Results of the static pressure, total pressure and time mean velocity (by x-wire probe)

α	y	y/y_{\max}	ΔP_{st-R}	ΔP_{tot-R}	\bar{U}_{PIT}	\bar{U}_C	\bar{U}	Ψ_D	\bar{V}_{TR}/\bar{U}
grad	mm	1	torr	torr	$m \cdot s^{-1}$	$m \cdot s^{-1}$	$m \cdot s^{-1}$	grad	1
-60	1,5	0,148	2,440	1,100	28,8	31,72	27,40	85,90	0,5832
	2,0	0,197	1,980	1,310	28,1	33,11	29,14	88,63	0,5396
	3,0	0,296	1,315	1,780	27,2	31,34	28,73	84,95	0,4354
	4,0	0,395	0,870	2,020	26,3	29,44	27,63	82,18	0,3674
	6,0	0,592	0,430	2,180	25,1	27,19	26,42	70,11	0,2445
	7,0	0,691	0,295	2,210	24,6	27,01	(26,60)	79,37	0,1747
	8,0	0,790	0,210	2,230	24,1	25,63	25,31	47,78	0,1587
<hr/>									
-50	1,5	0,134	2,475		28,6	30,72	26,27	85,34	0,6070
	2,0	0,178	2,050		27,8	32,43	27,99	88,81	0,5850
	3,0	0,268	1,370		26,9	30,67	27,65	87,45	0,4805
	4,0	0,357	0,935		26,0	29,07	27,00	83,11	0,4000
	6,0	0,535	0,445		25,1	26,97	26,03	75,86	0,2721
	8,0	0,714	0,200		24,2	25,52	25,10	60,75	0,1833
	9,5	0,847	0,105		23,2	24,63	24,38	38,68	0,1433
<hr/>									
-40	1,5	0,123	2,520		28,4	31,10	26,34	86,49	0,6279
	2,0	0,164	2,115		27,7	33,07	28,28	88,24	0,6071
	3,0	0,247	1,410		26,8	31,35	27,90	86,11	0,5132
	4,0	0,329	0,980		26,0	29,78	27,29	85,92	0,4372
	6,0	0,493	0,475		25,1	27,63	26,44	81,48	0,3042
	8,0	0,658	0,210		24,2	26,34	25,78	68,85	0,2089
	10,0	0,822	0,080		23,1	24,91	24,66	45,17	0,1428
<hr/>									

α	y	y/y_{\max}	Δp_{st-R}	Δp_{tot-R}	\bar{U}_{PIT}	\bar{U}_C	\bar{U}	Ψ_D	\bar{V}_{TR}/\bar{U}
grad	mm	1	torr	torr	m. s ⁻¹	m. s ⁻¹	m. s ⁻¹	grad	1
- 30	1,5	0,116	2520	0,900	28,50	29,00	24,76	85,22	0,6105
	2,0	0,155	2140	1,120	27,80	32,39	27,47	89,32	0,6247
	3,0	0,232	1,470	1,560	27,00	31,10	27,51	88,06	0,5277
	4,0	0,309	1,035	1,870	26,25	29,61	27,06	84,53	0,4448
	6,0	0,464	0,510	2,150	25,15	27,25	25,96	76,84	0,3190
	8,0	0,618	0,230	2,250	24,20	25,90	25,35	76,11	0,2115
	10,0	0,773	0,080	2,190	23,20	24,68	24,51	62,77	0,1201
	11,0	0,850	0,045	2,140	22,70	24,39	24,27	39,88	0,1044
<hr/>									
- 20	1,5	0,111	2560		29,10	29,22	25,55	81,38	0,5545
	2,0	0,148	2,190		28,30	33,39	28,44	86,66	0,6150
	3,0	0,222	1,505		27,60	31,59	27,54	86,68	0,5611
	4,0	0,296	1,070		26,75	30,06	27,04	85,68	0,4855
	6,0	0,444	0,510		25,10	27,57	25,99	84,37	0,3539
	8,0	0,592	0,225		24,10	26,24	25,48	82,34	0,2468
	10,0	0,740	0,080		23,35	25,35	25,06	78,64	0,1488
	12,0	0,888	0,010		22,55	24,23	24,14	40,06	0,0845
<hr/>									
- 10	1,5	0,108	2,610		30,40	28,52	24,18	84,52	0,6253
	2,0	0,144	2,200		29,50	33,10	27,39	89,96	0,6786
	3,0	0,216	1,545		28,40	31,53	27,30	88,42	0,5781
	4,0	0,288	1,100		27,20	30,22	27,22	85,75	0,4834
	6,0	0,432	0,540		25,10	27,63	26,12	79,40	0,3445
	8,0	0,576	0,255		24,00	26,18	25,44	78,62	0,2426
	10,0	0,721	0,110		23,50	25,29	25,04	77,01	0,1491
	12,0	0,865	0,020		22,70	24,10	24,00	45,18	0,0835

α	y	y/y_{\max}	Δp_{st-R}	Δp_{tot-R}	\bar{U}_{PIT}	\bar{U}_c	\bar{U}	Ψ_D	\bar{V}_{TR}/\bar{U}
grad	mm	1	torr	torr	m. s ⁻¹	m. s ⁻¹	m. s ⁻¹	grad	1
0	1,5	0,107	2,620	1,58	31,4	—	—	77,81	0,5378
	2,0	0,143	2,210	1,73	30,8	32,76	28,91	93,04	0,5497
	3,0	0,214	1,615	1,91	29,0	31,01	28,11	96,73	0,4792
	4,0	0,286	1,165	2,04	27,5	29,73	27,59	97,29	0,4236
	6,0	0,429	0,565	2,10	25,1	27,38	26,27	94,18	0,3070
	8,0	0,571	0,290	2,15	24,1	26,15	25,55	86,65	0,2288
	10,0	0,714	0,145	2,24	23,7	25,44	25,17	85,52	0,1571
	12,0	0,857	0,040	2,17	23,0	24,32	24,26	72,59	0,0895
<hr/>									
+ 10	1,5	0,108	2,630		30,6	—	—	86,22	0,6721
	2,0	0,144	2,265		29,8	32,69	27,05	91,09	0,6789
	3,0	0,216	1,635		28,7	31,45	27,24	91,39	0,5775
	4,0	0,288	1,170		27,4	29,86	26,83	90,74	0,4884
	6,0	0,432	0,570		25,3	27,69	26,12	92,32	0,3512
	8,0	0,576	0,290		24,2	26,52	25,81	90,14	0,2367
	10,0	0,721	0,150		23,8	25,32	25,06	95,54	0,1455
	12,0	0,865	0,060		22,9	24,31	24,18	143,15	0,1044
<hr/>									
+ 20	1,5	0,111	2,620		29,7	30,20	25,26	87,65	0,6549
	2,0	0,148	2,240		28,7	33,15	27,78	91,22	0,6510
	3,0	0,222	1,610		27,8	31,56	27,72	91,38	0,5444
	4,0	0,296	1,160		27,1	30,17	27,39	91,97	0,4617
	6,0	0,444	0,580		25,3	27,88	26,41	91,92	0,3385
	8,0	0,592	0,285		24,3	26,83	26,13	95,44	0,2324
	10,0	0,740	0,135		23,9	26,05	25,78	106,95	0,1458
	12,0	0,888	0,080		22,9	24,57	24,40	155,20	0,1176

α	y	y/y_{max}	Δp_{st-R}	Δp_{tot-R}	\bar{U}_{PIT}	\bar{U}_C	\bar{U}	ψ_D	\bar{V}_{TR}/\bar{U}
grad	mm	1	torr	torr	m. s ⁻¹	m. s ⁻¹	m. s ⁻¹	grad	1
+ 30	1,5	0,116	2,605	0,900	29,0	30,23	25,56	87,72	0,6316
	2,0	0,155	2,210	1,070	28,0	33,70	28,53	92,65	0,6289
	3,0	0,232	1,585	1,560	27,3	32,12	28,42	93,49	0,5265
	4,0	0,309	1,130	1,880	26,8	30,17	27,38	92,59	0,4631
	6,0	0,464	0,550	2,170	25,4	28,17	26,71	93,18	0,3353
	8,0	0,618	0,255	2,270	24,4	27,07	26,41	99,39	0,2257
	10,0	0,773	0,110	2,280	23,9	26,36	26,13	114,80	0,1339
	11,0	0,850	0,065	2,240	23,3	25,50	25,32	141,80	0,1203
+ 40	1,5	0,123	2,710		28,9	30,62	26,12	85,83	0,6117
	2,0	0,164	2,240		27,9	33,30	28,19	90,94	0,6287
	3,0	0,247	1,490		27,2	31,76	28,05	91,99	0,5307
	4,0	0,329	1,025		26,8	30,05	27,47	93,86	0,4432
	6,0	0,493	0,500		25,4	28,11	26,90	100,06	0,3031
	8,0	0,658	0,235		24,5	27,03	26,52	110,71	0,1973
	10,0	0,822	0,110		23,7	25,74	25,48	139,40	0,1439
+ 50	1,5	0,134	2,770		29,2	31,81	27,04	90,17	0,6198
	2,0	0,178	2,240		28,1	33,44	28,84	93,71	0,5871
	3,0	0,268	1,455		27,3	31,81	28,67	95,07	0,4804
	4,0	0,357	1,000		26,6	30,06	27,92	95,89	0,3986
	6,0	0,535	0,435		25,3	27,94	27,01	100,55	0,2645
	8,0	0,714	0,210		24,4	26,80	26,45	116,10	0,1637
	9,0	0,803	0,150		23,8	26,24	26,01	132,30	0,1325
	9,5	0,847	0,130		23,5	25,93	25,73	144,10	0,1255

α	y	y/y_{\max}	Δp_{st-R}	Δp_{tot-R}	\bar{U}_{PIT}	\bar{U}_C	\bar{U}	Ψ_D	\bar{V}_{TR}/\bar{U}
grad	mm	1	torr	torr	$m \cdot s^{-1}$	$m \cdot s^{-1}$	$m \cdot s^{-1}$	grad	1
+ 60	1,5	0,148	2500	1,130	29,6	32,81	27,85	90,16	0,6226
	2,0	0,197	2090	1,340	28,6	32,97	28,72	94,39	0,5641
	3,0	0,296	1,395	1,800	27,6	31,33	28,45	96,03	0,4609
	4,0	0,395	0,910	2,060	26,7	29,77	27,80	97,77	0,3827
	5,0	0,494	0,620	2,190	25,2	28,76	27,50	100,30	0,3063
	6,0	0,592	0,410	2,260	24,2	27,93	27,18	105,20	0,2371
	7,0	0,691	0,280	2,280	23,5	27,25	26,83	114,80	0,1784
	8,0	0,790	0,200	2,270	22,8	26,44	26,14	135,20	0,1515
	8,5	0,839	0,175	2,240	21,2	25,94	25,65	148,90	0,1506
+ 70	1,5	0,167	2,540		30,1	33,54	28,86	90,81	0,5919
	2,0	0,223	2,070		29,0	33,37	29,40	94,06	0,5368
	3,0	0,335	1,305		27,8	31,60	29,06	96,09	0,4273
	4,0	0,446	0,870		26,6	29,77	28,16	99,51	0,3431
	5,0	0,558	0,610		25,7	28,67	27,63	105,40	0,2769
	6,0	0,670	0,430		25,0	27,83	27,20	117,20	0,2173
	7,0	0,781	0,310		24,4	26,98	26,56	136,00	0,1788
+ 80	1,5	0,194	2,580		30,6	34,93	30,87	93,70	0,5297
	2,0	0,258	1,970		29,5	34,26	31,03	96,44	0,4681
	3,0	0,388	1,240		27,9	31,64	29,78	99,24	0,3594
	4,0	0,517	0,800		26,5	29,96	28,92	104,80	0,2712
	5,0	0,646	0,560		25,6	28,67	28,06	122,50	0,2099
	6,0	0,775	0,440		24,8	27,48	27,04	143,00	0,1819

α	y	y/y_{\max}	$-\Delta p_{st-R}$	Δp_{tot-R}	\bar{U}_{PIT}	\bar{U}_C	\bar{U}	Ψ_D	\bar{V}_{TR}/\bar{U}
grad	mm	1	torr	torr	m. s ⁻¹	m. s ⁻¹	m. s ⁻¹	grad	1
+ 90	1,5	0,230	2,420	1,420	31,0	36,23	32,54	93,42	0,4893
	2,0	0,307	1,950	1,710	29,8	34,78	32,01	95,42	0,4251
	3,0	0,461	1,200	2,060	27,9	32,16	30,63	98,93	0,3198
	4,0	0,615	0,765	2,150	26,4	30,43	29,56	112,80	0,2444
	5,0	0,691	0,630	2,070	25,9	29,27	28,51	129,80	0,2321

7

TAB. 2

$\alpha = 0$		$Re = 1,794 \cdot 10^4$		Ψ_D [grad]				
$2y/y_{max}$	0,286	0,571	1,143	1,714				
x/d_h	Ψ_D	\bar{V}_{TR}/\bar{U}	Ψ_D	\bar{V}_{TR}/\bar{U}	Ψ_D	\bar{V}_{TR}/\bar{U}	Ψ_D	\bar{V}_{TR}/\bar{U}
0,0143	95,2	0,562	97,2	0,419	88,3	0,223	70,0	0,074
0,0500	93,9	0,527	98,3	0,401	—	—	—	—
0,0857	86,0	0,480	99,7	0,379	—	—	—	—
0,1214	60,9	0,454	100,6	0,357	90,9	0,195	70,1	0,065
0,1571	40,9	0,523	102,1	0,332	—	—	—	—
0,1929	28,1	0,600	102,9	0,308	—	—	—	—
0,2643	21,4	0,642	102,6	0,251	94,6	0,152	70,3	0,055
0,4071	15,8	0,529	62,6	0,190	99,5	0,111	67,1	0,044
0,5500	8,00	0,394	32,5	0,218	108,2	0,075	59,8	0,036

Tab.3: Results of flow direction measurements in the axial direction

$$\frac{e_k^2}{S^2} = a_{ij} (\psi_k) \cdot \overline{u_i u_j} \quad ; \quad i=1+3 ; j \geq i$$

WIRE (CHANNEL)	WIRE POSITION PROBE POS.	$a_{ij} (\psi)$					
		a_{11}	a_{22}	a_{33}	a_{12}	a_{13}	a_{23}
I	1 A	m		$\frac{p^2}{m}$		- 2 p	
	2 B	m	$\frac{1}{2} \cdot \frac{p^2}{m}$	$\frac{1}{2} \cdot \frac{p^2}{m}$	$-\frac{2}{\sqrt{2}} p$	$-\frac{2}{\sqrt{2}} p$	$\frac{p^2}{m}$
	3 C	m	$\frac{p^2}{m}$		- 2 p		
	4 D	m	$\frac{1}{2} \frac{p^2}{m}$	$\frac{1}{2} \frac{p^2}{m}$	$-\frac{2}{\sqrt{2}} p$	$\frac{2}{\sqrt{2}} p$	$-\frac{p^2}{m}$
	5 A	m		$\frac{p^2}{m}$		2 p	
	6 B	m	$\frac{1}{2} \frac{p^2}{m}$	$\frac{1}{2} \frac{p^2}{m}$	$\frac{2}{\sqrt{2}} p$	$\frac{2}{\sqrt{2}} p$	$\frac{p^2}{m}$
	7 C	m	$\frac{p^2}{m}$		2 p		
	8 D	m	$\frac{1}{2} \cdot \frac{p^2}{m}$	$\frac{1}{2} \cdot \frac{p^2}{m}$	$\frac{2}{\sqrt{2}} p$	$-\frac{2}{\sqrt{2}} p$	$-\frac{p^2}{m}$

$$m = \sin^2 \gamma + k^2 \cdot \cos^2 \gamma$$

$$p = \sin \gamma \cdot \cos \gamma (1 - k^2)$$

Tab. 4: Resulting set of equations

$b_{ij} (\psi)$	WIRE POS.	$\frac{(e_k \pm e_{k+4})^2}{S} = b_{ij} (\psi) \cdot \bar{u}_i \cdot \bar{u}_j$					
		k	b_{11}	b_{22}	b_{33}	b_{12}	b_{13}
$\frac{(e_k + e_{k+4})^2}{S}$	1		n_{15}^2		\bar{q}_{51}^2		$2 \cdot n_{15} \cdot \bar{q}_{51}$
	2		n_{26}^2	$\frac{1}{2} \cdot \bar{q}_{62}^2$	$\frac{1}{2} \cdot \bar{q}_{62}^2$	$\frac{2}{\sqrt{2}} n_{26} \cdot \bar{q}_{62}$	$\frac{2}{\sqrt{2}} n_{26} \cdot \bar{q}_{62}$
	3		n_{37}^2	\bar{q}_{73}^2		$2 \cdot n_{37} \cdot \bar{q}_{73}$	
	4		n_{48}^2	$\frac{1}{2} \cdot \bar{q}_{48}^2$	$\frac{1}{2} \cdot \bar{q}_{84}^2$	$\frac{2}{\sqrt{2}} n_{48} \cdot \bar{q}_{84}$	$-\frac{2}{\sqrt{2}} n_{48} \cdot \bar{q}_{84}$
$\frac{(e_k - e_{k+4})^2}{S^2}$	1		\bar{n}_{15}^2		q_{15}^2		$-2 \bar{n}_{15} \cdot q_{15}$
	2		\bar{n}_{26}^2	$\frac{1}{2} \cdot q_{26}^2$	$\frac{1}{2} \cdot q_{26}^2$	$-\frac{2}{\sqrt{2}} \bar{n}_{26} \cdot q_{26}$	$-\frac{2}{\sqrt{2}} \bar{n}_{26} \cdot q_{26}$
	3		\bar{n}_{37}^2	q_{37}^2		$-2 \bar{n}_{37} \cdot q_{37}$	
	4		\bar{n}_{48}^2	$\frac{1}{2} \cdot q_{48}^2$	$\frac{1}{2} \cdot q_{48}^2$	$-\frac{2}{\sqrt{2}} \bar{n}_{48} \cdot q_{48}$	$\frac{2}{\sqrt{2}} \bar{n}_{48} \cdot q_{48}$

Tab.5: Resulting set of equations

$\alpha = 0$ $x/d_h = 0,05$ $Re = 1,794 \cdot 10^4$

y [mm]	$\frac{2y}{y_{max}}$	$\frac{u'}{v^*}$	$\frac{v'}{v^*}$	$\frac{w'}{v^*}$	$\frac{u'v'}{v^{*2}}$	$\frac{u'w'}{v^{*2}}$	$\frac{v'w'}{v^{*2}}$	$\frac{k'}{v^{*2}}$
2,0	0,286	1,0647	1,0004	1,3434	-1,1037	-0,4600	0,7071	1,9696
3,0	0,429	0,5881	0,6853	0,8028	-0,3263	-0,2286	0,2840	0,7300
4,0	0,571	0,3998	0,5326	0,4509	-0,1183	-0,0332	0,0430	0,3234
5,0	0,714	0,2855	0,4177	0,3842	-0,0381	-0,0161	-0,0037	0,2018
6,5	0,929	0,3115	0,4021	0,3421	-0,0656	-0,0065	-0,0002	0,1879
8,0	1,143	0,3846	0,4777	0,3878	-0,0994	-0,0082	0,0293	0,2632
9,0	1,286	0,3715	0,4491	0,3548	-0,0785	0,0247	0,0594	0,2328
10,0	1,429	0,3958	0,4615	0,3509	-0,0198	0,0569	0,0502	0,2464
11,0	1,571	0,4292	0,5071	0,3836	0,0329	0,0459	0,0136	0,2943
12,0	1,714	0,5206	0,5297	0,5390	0,0460	0,0207	-0,0113	0,4211
12,4	1,771	0,4885	0,4317	0,5432	0,0422	0,0186	0,0207	0,3600

Tab. 6: Results of the fluctuation measurements along the line
 $x/d_h = 0,05, \alpha = 0$

$\alpha = 0$		$Re = 1,794 \cdot 10^4$			$v^* = 1,5236 \text{ m/s}$				
x/d_h	$2y/y_{max}$	$\frac{u'}{v^*}$	$\frac{v'}{v^*}$	$\frac{w'}{v^*}$	$\frac{u'v'}{v^*}$	$\frac{u'w'}{v^*}$	$\frac{v'w'}{v^*}$	$\frac{k'}{v^*}$	
0,0143	0,2857	0,8922	0,7810	1,3064	-0,7704	0,4869	0,6417	1,5563	
0,0500		1,0647	1,0004	1,3434	-1,1037	-0,4600	0,7071	1,9696	
0,1214		—	—	—	—	—	—	—	
0,2643		3,0526	2,3865	1,9236	-0,2493	2,2146	1,4985	9,3570	
0,4071		2,8417	1,6994	2,1897	-1,0092	4,1393	-0,4459	6,9208	
0,5500		2,3260	1,6950	1,1760	—	1,4600	0,5930	4,833	
0,0143	0,5714	0,3772	0,4929	0,4101	-0,0911	-0,0196	0,0251	0,2767	
0,0500		0,3998	0,5326	0,4509	-0,1183	-0,0332	0,0430	0,3234	
0,1214		0,4965	0,6347	0,6398	-0,1997	-0,1017	0,1516	0,5294	
0,2643		0,8196	0,8192	1,1626	-0,3592	-0,4761	0,4797	1,3472	
0,4071		1,3768	0,9304	1,7218	0,0875	-1,1924	0,3517	2,8629	
0,5500		1,9795	1,5714	1,9100	-0,8482	-2,2560	0,7121	5,0021	
0,0143	1,1430	0,3872	0,4782	0,3916	-0,1029	-0,0028	0,0326	0,2660	
0,0500		0,3846	0,4777	0,3878	-0,0994	-0,0082	0,0293	0,2632	
0,1214		0,3823	0,4790	0,4180	-0,0920	-0,0156	0,0247	0,2752	
0,2643		0,3811	0,4790	0,4297	-0,0742	-0,0100	0,0051	0,2797	
0,4071		0,3824	0,4768	0,4455	-0,0511	-0,0025	-0,0044	0,2860	
0,5500		0,3955	0,4839	0,4759	-0,0331	-0,0054	-0,0068	0,3085	
0,0143	1,7140	0,5262	0,5331	0,5453	0,0463	0,0206	-0,0104	0,4292	
0,0500		0,5206	0,5297	0,5390	0,0460	0,0207	-0,0113	0,4211	
0,1214		0,5110	0,5283	0,5268	0,0449	0,0221	-0,0095	0,4089	
0,2643		0,4868	0,5146	0,4797	0,0406	0,0292	-0,0009	0,3659	
0,4071		0,4730	0,5153	0,4644	0,0413	0,0327	0,0083	0,3525	
0,5500		0,4604	0,5070	0,4727	0,0447	0,0194	0,0028	0,3462	

Tab. 7: Results of the fluctuation measurements in the axial direction